

Supporting Information

Highly efficient orange OLEDs with narrow-emitting symmetric tetradentate platinum (II) complexes based on rigid steric hinderance aza-triptycene pyridazine ligands

Qunbo Mei,^{*a†} Xueyan Ma,^{†a} Beibei Qiu,^a You Zhai,^a Lanlan Zhao,^a Nianshu Li,^a Bihai Tong^{*b}

^aKey Laboratory for Organic Electronics and Information Displays (KLOEID) & Institute of Advanced Materials (IAM), Jiangsu National Synergistic Innovation Center for Advanced Materials (SICAM), Nanjing University of Posts & Telecommunications, Nanjing, 210023, China. E-mail: iamqbmei@njupt.edu.cn

^bKey Laboratory of Metallurgical Emission Reduction & Resources Recycling, Ministry of Education, School of Metallurgy Engineering, Anhui University of Technology, Maanshan, 243002, Anhui, China. E-mail: tongbihai@163.com

[†] Authors contributed equally. * Corresponding authors.

Contents:

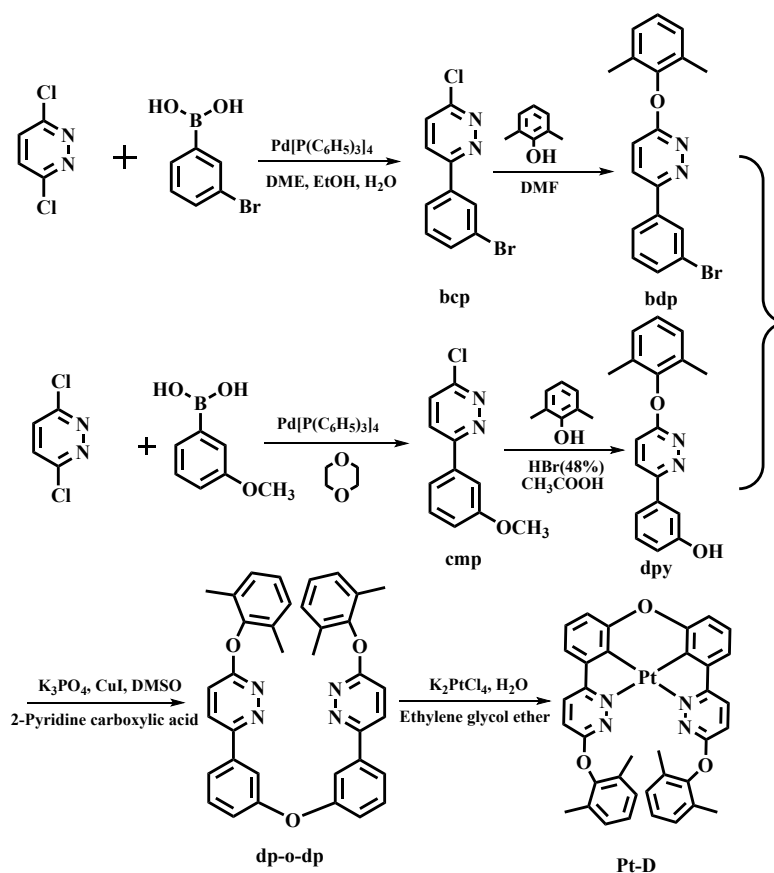
1. **General descriptions**
2. **Fig. S1** The full width at half maximum of the emission maxima of these complexes.
3. **Fig. S2** The PL spectra of complexes **Pt-DPM**, **Pt-PIP** and **Pt-DPT** in PMMA films at a conc. of 1 wt % at (a) room temperature and (b) 77K.
4. **Fig. S3** The PL spectra of complexes **Pt-DPM** and **Pt-D** in (a) CH₂Cl₂ solution and (b) PMMA at room temperature.
5. **Fig. S4** Life decay diagram of complexes doped in 1 wt % PMMA.
6. **Fig. S5** (a) EL spectra at 8V. (b) Current density and luminance as a function of applied voltage. (c) Luminance efficiencies. (d) EQE of devices based on complex **Pt-DPM**. (e) CIE coordinates dependence on the luminance of the devices **Pt-DPM**.
7. **Fig. S6** (a) EL spectra at 8V. (b) Current density and luminance as a function of applied voltage. (c) Luminance efficiencies. (d) EQE of devices based on complex **Pt-PIP**. (e) CIE coordinates dependence on the luminance of the devices **Pt-PIP**.
8. **Fig. S7** (a) EL spectra at 8V. (b) Current density and luminance as a function of applied voltage. (c) Luminance efficiencies. (d) EQE of devices based on complex **Pt-DPT**. (e) CIE coordinates dependence on the luminance of the devices **Pt-DPT**.
9. **Fig. S8** (a) Current density as a function of applied voltage. (b) Voltage efficiencies of devices based on complex **Pt-D**.
10. **Table S1** The photophysical properties of these complexes.
11. **Table S2** Performance of the devices based on new complexes.
12. ¹H NMR data of ligands **dda**, **ddcp**, **cdpm**, **cpip**, **cdpt**, **obb**, **obp**, **ODPM**, **OPIP**, **ODPT**, **bcp**, **bdp**, **cmp**, **dpy** and **dp-o-dp**. (**Fig. S9-Fig. S23**).
13. ¹H NMR data of complexes **Pt-DPM**, **Pt-PIP**, **Pt-DPT** and **Pt-D**. (**Fig. S24-Fig. S27**).
14. High resolution mass spectrometers (MALDI-TOF) of all new ligand and complexes **Pt-DPM**, **Pt-PIP**, **Pt-DPT** and **Pt-D**. (**Fig. S28-Fig. S31**).

15. ^{13}C NMR data of complexes **Pt-DPM**, **Pt-PIP** and **Pt-DPT**. (Fig. S32-Fig. S34).

1. General descriptions

1.1 Materials and characterization

The ^1H and ^{13}C NMR (δ in ppm) spectra were recorded on a Bruker Ultra Shield Plus 400 MHz spectrometer with TMS as the internal standard. Mass spectra were acquired by a Bruker Daltonics matrix-assisted laser desorption/ionization time-of-flight mass spectrometer (MALDI-TOF-MASS). UV-vis absorption spectra were recorded on a Shimadzu UV-3600 UV-Vis-NIR Spectrophotometer. Steady state fluorescence spectra were obtained with a Shimadzu RF-5301PC Fluorescence Spectrophotometer. Photoluminescence quantum yields were determined by using an integrating sphere. Lifetime studies were performed with Edinburgh FLSP920 photcounting system with a semiconductor laser as the excitation source. For the thin film quantum yields and lifetime data measurements, samples (1 mg) were first dissolved in 1 mL of DCM containing polymethyl methacrylate (PMMA) (20 mg^{-1}), and spin-coated onto the quartz slides at a speed of 1500 rpm for 60 s. Cyclic voltammetry (CV) measurements were carried out with a CHI660 electrochemical workstation (Shanghai Chenhua, China) utilizing the three electrode configuration consisting of a glassy carbon (working electrode), platinum wire (auxiliary electrode) and Ag/AgNO_3 (reference electrode) electrodes. The experiments were done in dry DCM using 0.1 M tetrabutylammonium hexafluorophosphate as supporting electrolyte at a scanning rate of 0.1V/s at room temperature. Ferrocene was selected as the standard.



Scheme S1 Synthetic routes of the reference platinum (II) complex **Pt-D**

3-(3-Bromophenyl)-6-chloropyridazine(bcp):

A 100 mL two-necked flask was charged with dichloropyridazine (1.5 g, 10 mmol), 3-bromophenylboronic acid (2.58 g, 13 mmol), and potassium carbonate (2.07 g, 15 mmol). Tetrakis(triphenylphosphine)palladium (0.57 g) was added, followed by three evacuation-nitrogen backfilling cycles. Under nitrogen atmosphere, deoxygenated ethylene glycol dimethyl ether (25 mL), ethanol (10 mL) and water (11 mL) were introduced. The reaction proceeded at 120°C for 24 h. After cooling, the mixture was extracted with dichloromethane, and the organic layer was collected. Solvent removal via rotary evaporation was followed by gradient elution using petroleum ether and ethyl acetate (3:1, v/v) to afford 1.79 g **bcp** (6.7 mmol, 67%) of the product as a white solid. ¹H NMR (400 MHz, DMSO) δ = 8.43-8.38 (m, 1H), 8.32 (t, J =1.8, 1H), 8.15 (ddd, J =7.9, 1.6, 1.0, 1H), 8.04 (d, J =9.1, 1H), 7.75 (ddd, J =8.0, 2.0, 0.9, 1H), 7.52 (t, J =7.9, 1H).

3-(3-Bromophenyl)-6-(2,6-dimethylphenoxy) pyridazine (bdp):

A 100 mL two-necked flask was charged with **bcp** (1.3 g, 5 mmol), 2,6-dimethylphenol (1.23 g, 10 mmol) and potassium carbonate (2.07 g, 15 mmol). The flask was evacuated and backfilled with nitrogen three times. Dry DMF (15 mL) was added, and the reaction proceeded at 120°C for 24 h. Upon cooling, the mixture was quenched with ice-water, affording a precipitate. The precipitate was collected via suction filtration and purified by silica gel column chromatography using petroleum ether and ethyl acetate (5:1, v/v) as the eluent, yielding 0.93 g (52.5%) of the product **bdp** as a white solid. ¹H NMR(400 MHz, DMSO) δ = 8.37 (d, J =9.3, 1H), 8.25 (t, J =1.8, 1H), 8.07 (d, J =8.1, 1H), 7.68 (dd, J =8.0, 1.1, 1H), 7.58 (d, J =9.3, 1H), 7.48 (t, J =7.9, 1H), 7.16 (s, 2H), 7.12 (dd, J =8.8, 5.8, 1H), 2.06 (s, 6H).

3-Chloro-6-(3-methoxyphenyl) pyridazine (cmp):

A 100 mL two-necked flask was charged with dichloropyridazine (1.5 g, 10 mmol), 3-methoxyphenylboronic acid (1.96 g, 13 mmol) and potassium phosphate (1.4 g, 20 mmol). Pd₂(dba)₃ (0.12 g) and S-Phos (0.2 g) were added, followed by three evacuation-nitrogen purging cycles. Dry 1,4-dioxane (20 mL) was introduced, and the reaction proceeded at 100°C for 36 h. After cooling, the mixture was extracted with dichloromethane (DCM), and the organic layer was collected. Solvent removal via rotary evaporation was followed by silica gel column chromatography using petroleum ether and ethyl acetate (3:1, v/v), yielding 1.44 g (63.6%) of the product **cmp** as a white solid. ¹H NMR (400 MHz, DMSO) δ = 8.34 (d, J =9.1, 1H), 8.00 (d, J =9.1, 1H), 7.72-7.66 (m, 2H), 7.47 (t, J =8.0, 1H), 7.11 (dd, J =7.7, 2.4, 1H), 3.84 (s, 3H).

3-(6-(2,6-Dimethylphenoxy) pyridazin-3-yl) phenol (dpy):

A 100 mL two-necked flask was charged with **cmp** (1.1 g, 5 mmol), 2,6-dimethylphenol (1.23 g, 10 mmol) and potassium carbonate (2.07 g, 15 mmol). The flask was evacuated and backfilled with nitrogen three times. Dry DMF (15 mL) was added under nitrogen atmosphere, and the reaction proceeded at 120°C for 24 h. Upon cooling, the mixture was poured into ice water, affording a precipitate collected via suction filtration and purified by silica gel column chromatography. The isolated product was transferred to a fresh 100 mL two-necked flask. Under nitrogen protection, deoxygenated acetic acid (15 mL) was added, followed by 48% hydrobromic acid (2.4 mL). The reaction proceeded at 120°C for 24 h. After cooling, the pH was adjusted to weakly alkaline with potassium carbonate solution. A white solid **dpy** was isolated via suction filtration, yielding

48.5%. ¹H NMR (400 MHz, DMSO) δ = 9.66 (s, 1H), 8.21 (d, *J*=9.3, 1H), 7.50 (d, *J*=9.3, 1H), 7.47-7.40 (m, 2H), 7.29 (t, *J*=7.9, 1H), 7.16 (d, *J*=6.7, 2H), 7.11 (dd, *J*=8.7, 5.9, 1H), 6.87 (d, *J*=8.0, 1H), 2.06 (s, 6H).

6,6'-(Oxybis(3,1-phenylene)) bis (3-(2,6-dimethylphenoxy) pyridazine) (dp-o-dp):

A 50 mL conical flask was charged with **bdp** (0.35 g, 1 mmol), **dp** (0.38 g, 1.3 mmol), CuI (38 mg, 0.2 mmol), K₃PO₄ (0.56 g), and 2-pyridinecarboxylic acid (38 mg). The flask was evacuated and backfilled with nitrogen three times. Dry DMSO (15 mL) was added under N₂ protection, and the reaction proceeded at 120 °C for 24 h. After cooling, the mixture was extracted with dichloromethane, and the organic layer was collected. The solvent was removed by rotary evaporation, and the residue was purified by column chromatography with petroleum ether (PE) and ethyl acetate (EA) mixture (5:1, v/v) as the eluent. The product **dp-o-dp** was obtained as a white solid (0.213 g, 37.6% yield). ¹H NMR (400 MHz, DMSO) δ = 7.87 (d, *J*=9.3, 2H), 7.38 (d, *J*=8.1, 2H), 7.31-7.28 (m, 2H), 7.12-7.06 (m, 4H), 6.74 (dd, *J*=7.9, 2.0, 2H), 6.70-6.67 (m, 4H), 6.64 (dd, *J*=8.9, 5.6, 2H), 1.57 (s, 12H).

The reference platinum (II) complex (Pt-D)

A mixture of acetic acid (5 mL), K₂PtCl₄ (0.023 g, 0.055 mmol), tetrabutylammonium bromide (TBAB) (0.002g, 0.005 mmol) and the cyclometalated ligand **dp-o-dp** (0.028g, 0.05 mmol) was added to a Schlenk tube under an N₂ atmosphere. The reaction was stirred at room temperature for 12 h and then stirred at 120 °C for 70 h. The reaction mixture was cooled to room temperature and poured into 50 mL water. The residue was purified by column chromatography on silica gel using PE and DCM (1:1, v/v) as the eluent to afford the desired complexes **Pt-D**: Red solid. ¹H NMR (400 MHz, CDCl₃) δ = 8.01 (d, *J*=9.3, 2H), 7.37 (d, *J*=7.0, 1H), 7.32-7.31 (m, 1H), 7.29 (s, 1H), 7.11 (d, *J*=7.2, 3H), 7.08 (s, 1H), 7.03 (d, *J*=7.1, 2H), 2.25 (s, 6H). MALDI-TOF-MS (*m/z*): calcd for [M]⁺ C₃₆H₂₈N₄O₃Pt: 759.18, found: 758.31.

Dimethyl 9,10-dihydro-9,10-ethenoanthracene-11,12-dicarboxylate (ddcme)

A mixture of anthracene (7.5 g, 27.4 mmol) and DMAD (7.5 mL, 61 mmol) were added to a two-necked flask under an N₂ atmosphere. The reaction was stirred at 170 °C for 45 min and then stirred at 180 °C for 5 min. After cooling to room temperature, it was recrystallized from methanol as a white solid 8.0 g. Yield 91.2%. ¹H NMR (400 MHz, CDCl₃) δ 7.65 (s, 4H), 7.21 (s, 4H), 5.26 (s, 2H), 3.61 (s, 6H).

9,10-Dihydro-9,10-ethenoanthracene-11,12-dicarboxylic acid (ddca)

A mixture of **ddcme** (8 g, 27 mmol), NaOH (4 g, 100 mmol), CH₃OH (50 mL) and H₂O (15 mL) was stirred at 90 °C for 1 h. Then the reaction mixture was cooled to room temperature and poured into 500 mL water and adjusted the pH with dilute HCl acid to weak acidic. The precipitate was collected by filtration, dried for 24 h to give a white solid 6.89 g. Yield 94.4%. ¹H NMR (400 MHz, CDCl₃) δ 16.86 (s, 2H), 7.31 (s, 4H), 7.19 (s, 4H), 4.88 (s, 2H).

9,10-Dihydro-9,10-[3,4]furananthracene-12,14-dione (dda)

A mixture of **ddca** (6.89 g, 23.6 mmol), CH₃COONa (0.3 g, 3.7 mmol) and acetic anhydride (25 mL) was stirred at 80 °C for 0.5 h. Then the reaction mixture was cooled to room temperature

and remove the solvent in vacuo. The precipitate was collected by filtration, dried for 24 h to give a white solid 5.34 g. Yield 82%. $^1\text{H NMR}$ (400 MHz, CDCl_3) δ 7.45 (s, 4H), 7.09 (s, 4H), 5.55 (s, 2H).

9,10-Dihydro-9,10-[4,5]epipyridazinoanthracene-12,15-dione (dda)

A mixture of **dda** (5.34 g, 19.5 mmol) and CH_3COOH (30 mL) was stirred at 125 °C. After dissolving, the $\text{N}_2\text{H}_4 \cdot \text{H}_2\text{O}$ (3.5 g, 70 mmol) was slowly added to the reaction, and then stirred at 125 °C for 3 h. After cooling to room temperature, the precipitate was collected by filtration, dried for 24 h to give a yellow solid 4.38 g. Yield 78%. $^1\text{H NMR}$ (400 MHz, CDCl_3) δ 12.1 (s, 2H), 7.85 (s, 4H), 7.12 (s, 4H), 5.79 (s, 2H).

2.1 OLED fabrication and measurement

In a general procedure, indium tin oxide (ITO)-coated glass substrates were etched, patterned, and washed with detergent, deionized water, acetone, and ethanol in turn. For vacuum-deposited OLEDs, the ITO substrate was loaded in a deposition chamber and conducted with the treatment of ultraviolet ozone. Vacuum chambers were employed to deposit metal layer and organic layer, and the base pressure was higher than 8×10^{-5} Pa. For spin-coating OLEDs, PEDOT: PSS was spin-coated to smooth the ITO surface and to promote hole injection, and then the emissive layer was spin-coated from a chlorobenzene solution, on which an electron-transporting/hole-blocking layer and metal layer were deposited in a vacuum chamber at a pressure of 8×10^{-5} Pa. EL spectra were collected on a Spectra Scan PR655 photometer. Current density-voltage-luminance (J-V-L) measurements were recorded simultaneously using a Keithley 4200 semiconductor parameter analyzer coupled with a Newport Multi-Function 2835-C optical meter, which measured luminance in the forward direction. All device characterizations were carried out under ambient laboratory conditions at room temperature without encapsulation.

3.1 Materials and characterization

Commercially available reagents were used as received unless otherwise stated. X-ray crystallography diffraction was measured on a Bruker SMART Apex CCD diffractometer. Positive-ion ESI mass spectra were recorded with an AB Triple TOF 5600^{plus} mass spectrometer. Thermogravimetric analysis (TGA) was carried out on a Shimadzu DTG-60H thermogravimetric analyses under nitrogen flux at a heating rate of 10 °C min^{-1} . NMR spectra were measured on a Bruker Ultra Shield Plus 400 MHz spectrometer with TMS as the internal standard and CDCl_3 as the solvent. GC-MS was determined on a Shimadzu GC-MS-QP2010 Plus mass spectrometer, and electron spray ionization (ESI) mass spectra on a Thermo LCQDECAXP mass spectrometer. An Edinburgh FL920 time-correlated pulsed single-photon-counting instrument was employed to determine quantum efficiency. UV-vis absorption spectra and PL spectra were recorded using an UV-3600 Shimadzu and Shimadzu RF-5301PC fluorescence spectrophotometer, respectively. Cyclic voltammetry (CV) was recorded at a three-electrode electrochemical configuration which Pt disk electrode in HPLC grade dichloromethane solution containing 0.001 M of the platinum (II) complex, 0.1 M tetrabutylammonium hexafluorophosphate as the supporting electrolyte at a scanning rate of 0.1 $\text{V} \cdot \text{S}^{-1}$ at room temperature on a CHI660C spectrometer and Ag/AgNO_3 were used as the counter and reference electrodes. Ferrocene was selected as internal standard.

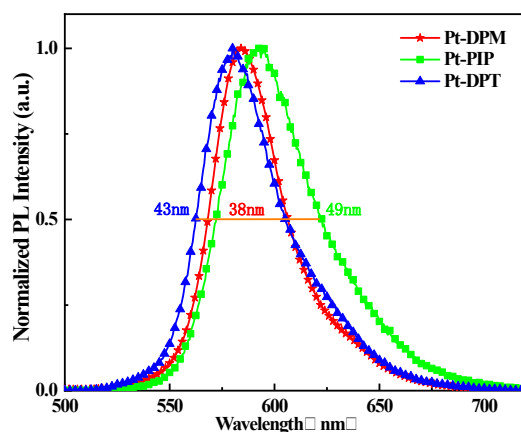


Fig. S1 The full width at half maximum of the emission maxima of these complexes.

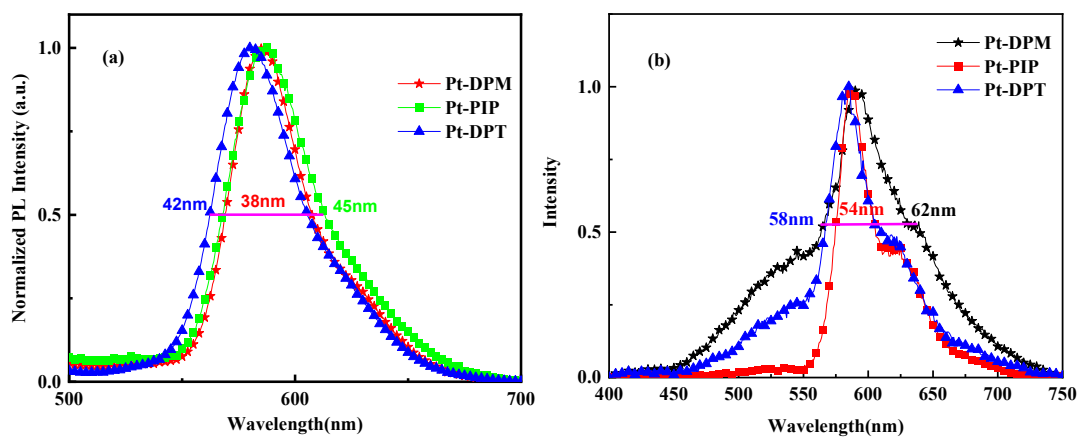


Fig. S2 The PL spectra of complexes **Pt-DPM**, **Pt-PIP** and **Pt-DPT** in PMMA films at a conc. of 1 wt % at (a) room temperature (The full width at half maximum of the emission maxima of these complexes are 38 nm, 45 nm and 42 nm respectively) and (b) 77K (The full width at half maximum of the emission maxima of these complexes is 62nm, 54nm and 58 nm respectively).

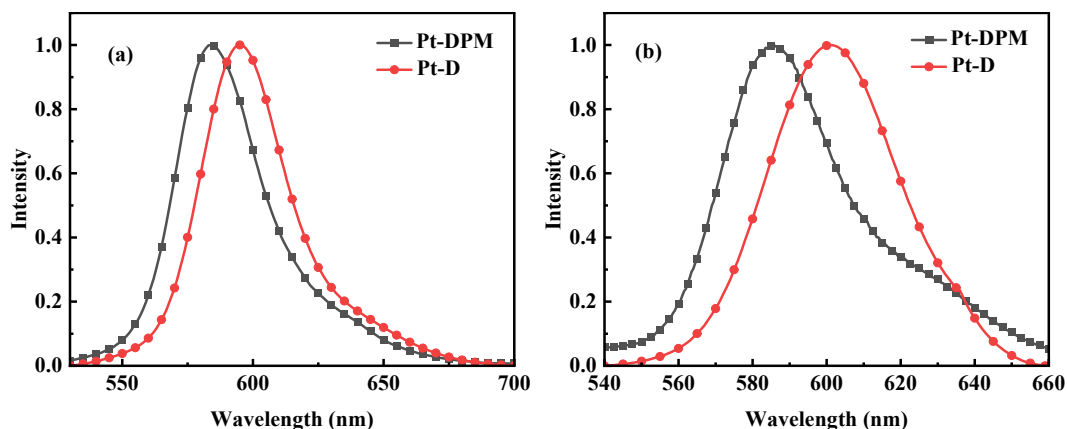


Fig. S3 The PL spectra of complexes **Pt-DPM** and **Pt-D** in (a) CH_2Cl_2 solution and (b) PMMA at room temperature.

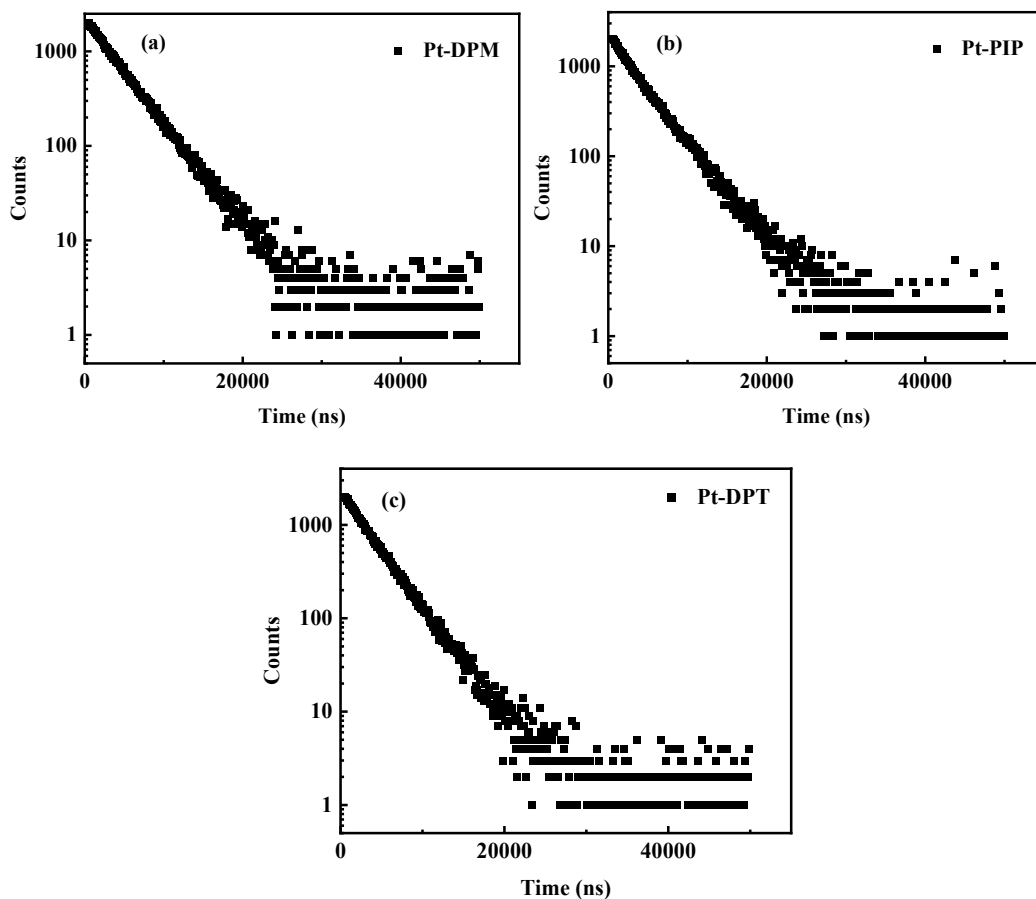
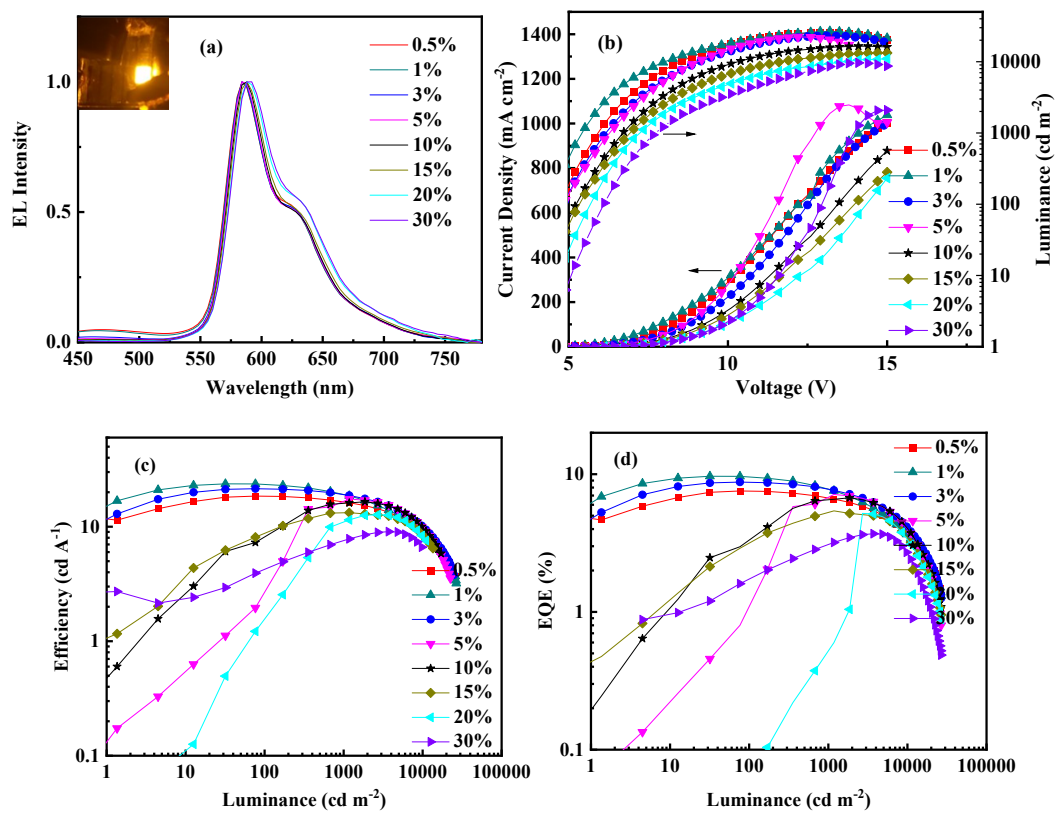


Fig. S4 Life decay diagram of complexes doped in 1 wt % PMMA.



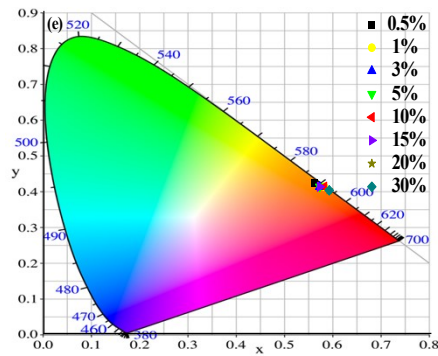


Fig. S5 (a) EL spectra at 8V. (b) Current density and luminance as a function of applied voltage. (c) Luminance efficiencies. (d) EQE of devices based on complex **Pt-DPM**. (e) CIE coordinates dependence on the luminance of the devices **Pt-DPM**.

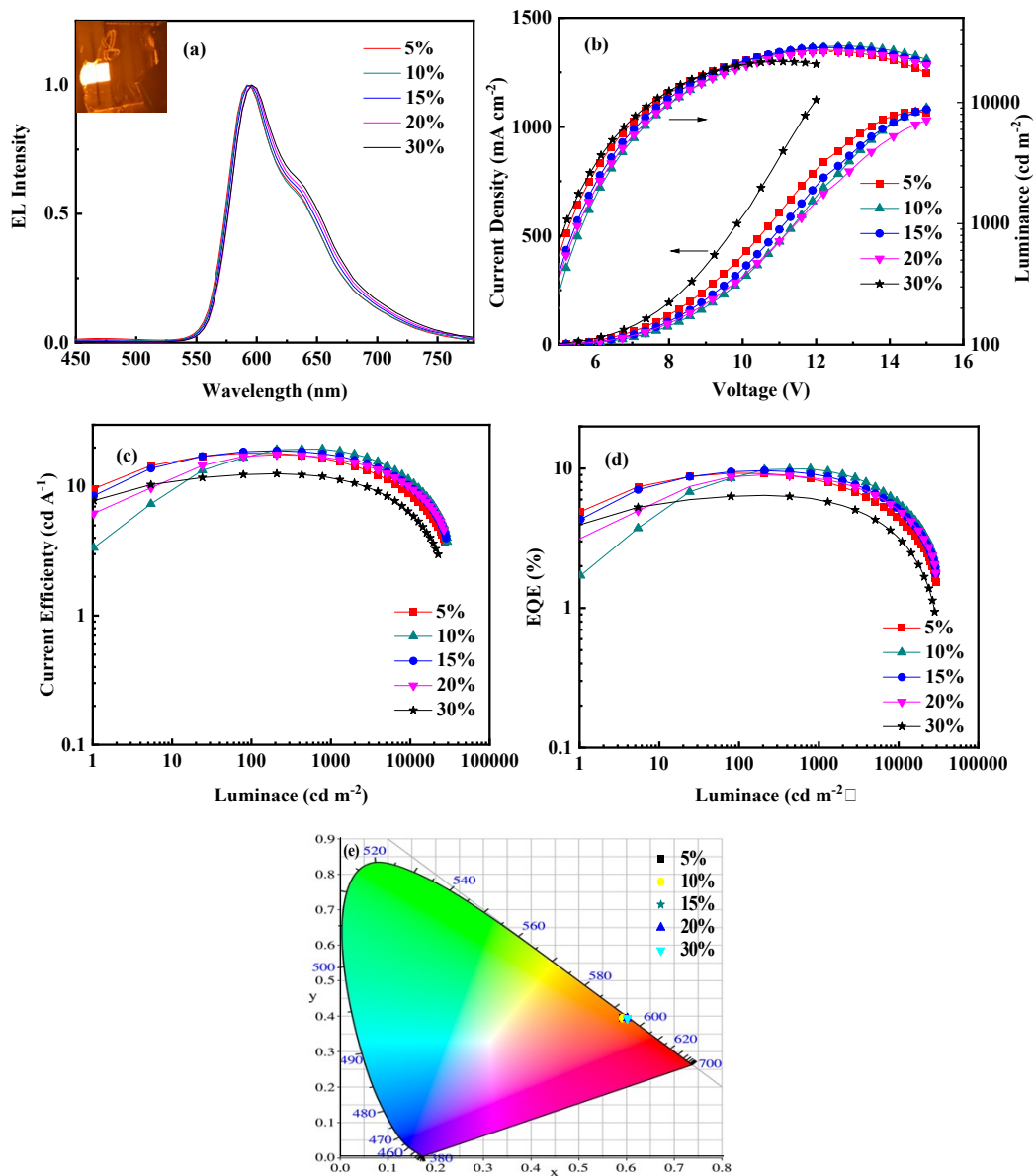


Fig. S6 (a) EL spectra at 8V. (b) Current density and luminance as a function of applied voltage. (c) Luminance efficiencies. (d) EQE of devices based on complex **Pt-PIP**. (e) CIE coordinates dependence on the luminance of the devices **Pt-PIP**.

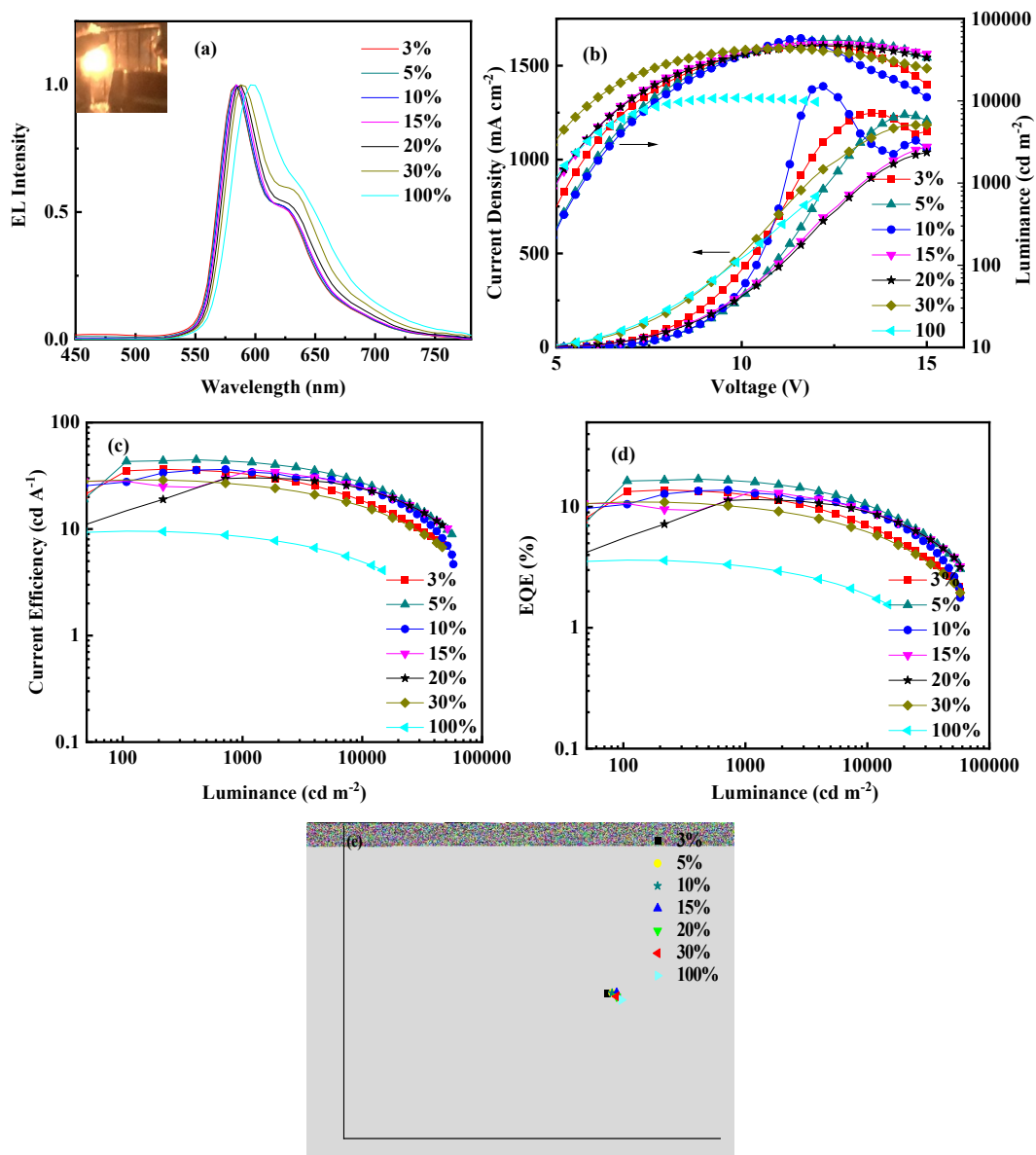


Fig. S7 (a) Current density and luminance as a function of applied voltage. (c) Luminance efficiencies. (d) EQE of devices based on complex **Pt-DPT**. (e) CIE coordinates dependence on the luminance of the devices **Pt-DPT**.

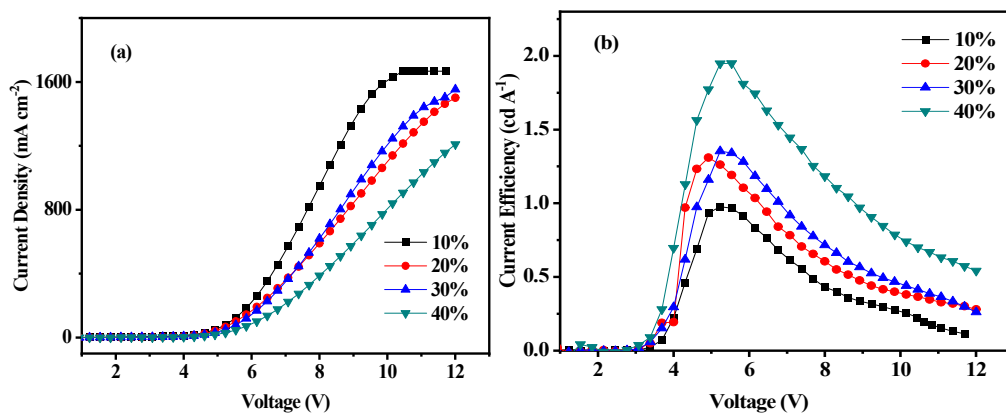


Fig. S8 (a) Current density as a function of applied voltage. (b) Voltage efficiencies of devices based on complex **Pt-D**.

Table S1 The photophysical properties of these complexes

Compounds	$\lambda_{\text{abs,max}}(\text{nm})$	$\lambda_{\text{em}}(\text{nm})^{\text{a}}$	$\lambda_{\text{em}}(\text{nm})^{\text{b}}$	$\lambda_{\text{em}}(\text{nm})^{\text{c}}$	$\tau(\mu\text{s})$
Pt-DPM	263,344,412	584	585	588	3.82
Pt-PIP	270,334,405	593	588	587	3.43
Pt-DPT	285,342,410	580	580	585	3.37
Pt-D	261,340,408	595	600	-	6.89

^a The PL spectra of complexes **Pt-DPM**, **Pt-PIP**, **Pt-DPT** and **Pt-D** in DCM at room temperature.

^b The PL spectra of complexes **Pt-DPM**, **Pt-PIP**, **Pt-DPT** and **Pt-D** in PMMA films at a conc. of 1 wt% at room temperature.

^c The PL spectra of complexes **Pt-DPM**, **Pt-PIP**, **Pt-DPT** and **Pt-D** in PMMA films at a conc. of 1 wt% at 77K.

Table S2 Performance of the devices based on new complexes

Dopant	Dopant level [wt %]	$\eta_{\text{c,max}}$ [cd A ⁻¹]	L_{max} [cd m ⁻²]	$\eta_{\text{p,max}}$ [lm W ⁻¹]	$\eta_{\text{EQE,max}}$ [%]	λ_{em} [nm]	CIE(x,y)	$V_{\text{turn-on}}$
Pt-DPM	0.5	18.51	25410	13.55	7.56	584	(0.56,0.42)	3.98
	1	23.67	26670	18.67	9.67	584	(0.58,0.41)	3.67
	3	21.46	23124	15.78	8.77	584	(0.57,0.41)	3.97
	5	17.46	22260	9.95	7.13	584	(0.57,0.41)	3.98
	10	16.52	16485	8.91	6.75	588	(0.58,0.41)	4.29
	15	13.27	13272	7.56	5.42	588	(0.57,0.41)	4.59
	20	12.71	11025	6.52	5.19	588	(0.59,0.40)	4.90
	30	9.05	9639	4.42	3.70	592	(0.59,0.40)	5.20
Pt-PIP	5	18.13	27048	10.18	9.25	592	(0.59,0.39)	3.67
	10	19.45	29232	11.08	9.93	592	(0.59,0.39)	3.98
	15	18.93	28392	12.13	9.66	596	(0.60,0.39)	4.29
	20	17.64	26208	11.30	9.00	596	(0.60,0.39)	4.59
	30	12.57	21756	8.02	6.42	596	(0.60,0.39)	4.31
Pt-DPT	3	36.39	48138	23.32	13.81	584	(0.56,0.42)	3.67
	5	44.66	54918	26.97	16.94	584	(0.57,0.42)	3.67
	10	36.35	57630	20.71	13.79	584	(0.57,0.42)	3.98
	15	36.06	49268	19.46	10.66	584	(0.58,0.42)	3.67
	20	30.32	46899	16.36	11.50	588	(0.58,0.41)	3.67
	30	28.92	43708	19.78	10.97	588	(0.58,0.41)	3.37
	30	28.92	43708	19.78	10.97	588	(0.58,0.41)	3.37
	100	9.56	10873	6.48	3.63	596	(0.59,0.40)	3.69

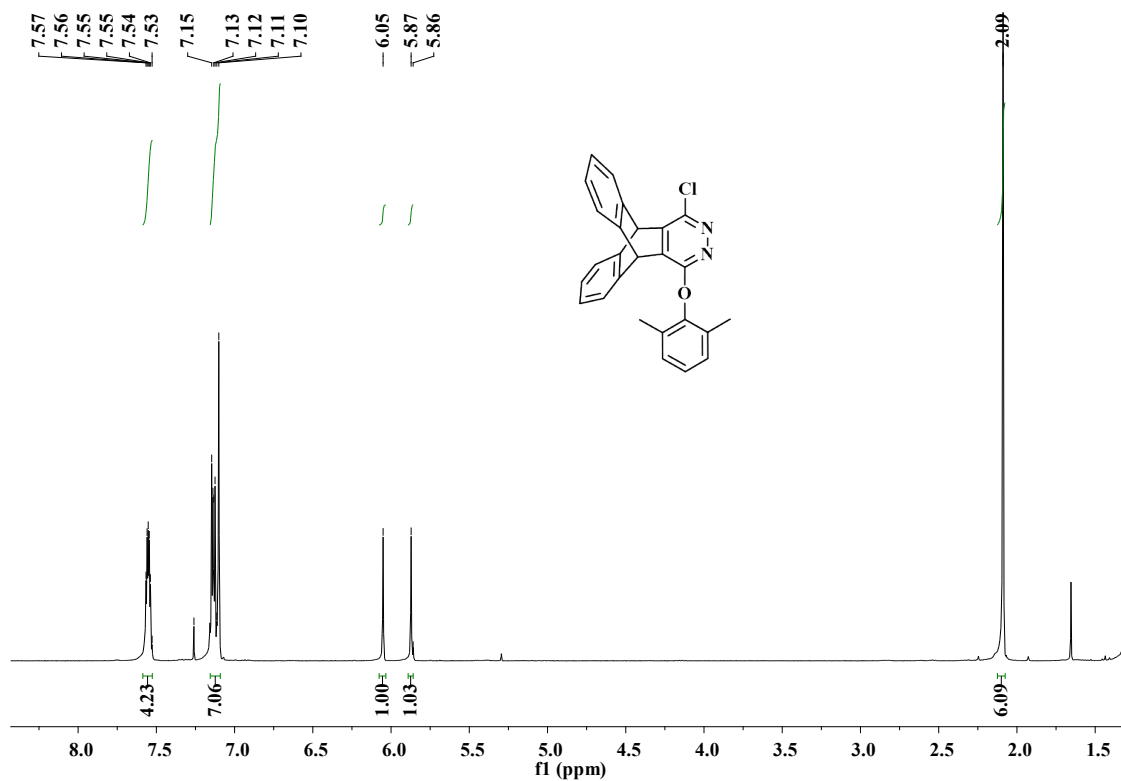


Fig. S11 $^1\text{H-NMR}$ spectrum of **cdpm** in *DMSO* (400 MHz)

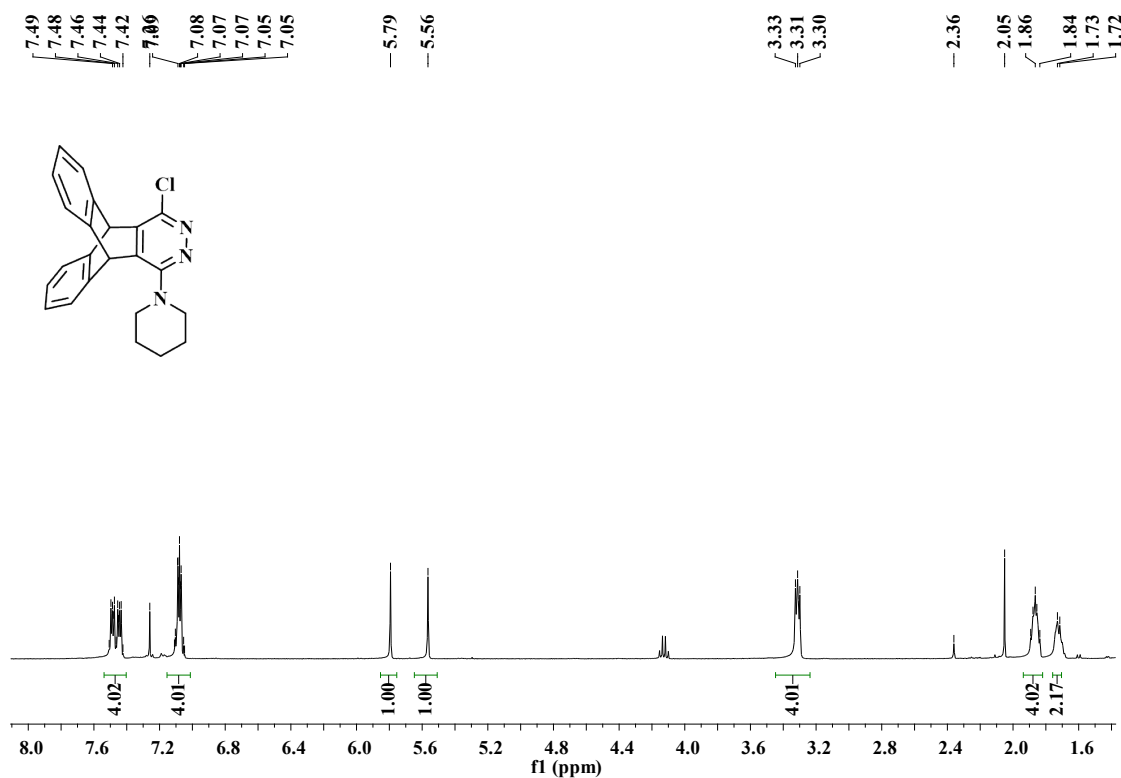


Fig. S12 $^1\text{H-NMR}$ spectrum of **cpip** in *CDCl₃* (400 MHz)

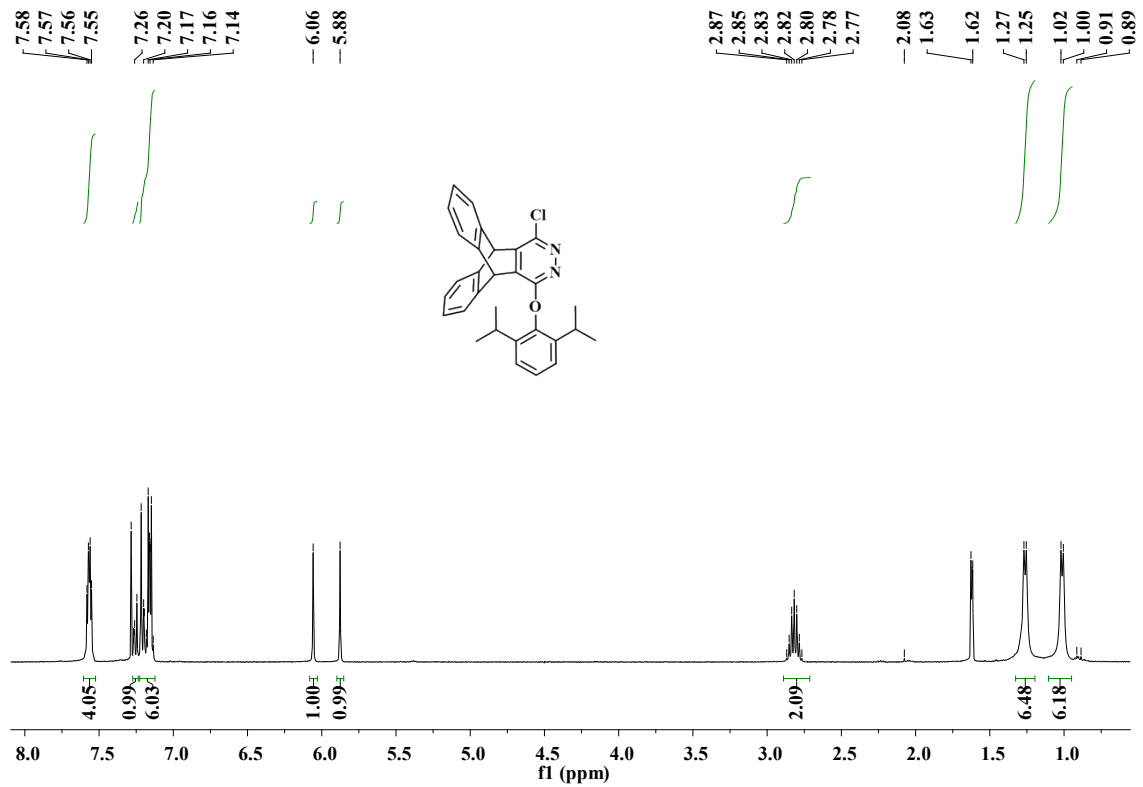


Fig. S13 ¹H-NMR spectrum of **cdpt** in CDCl₃ (400 MHz)

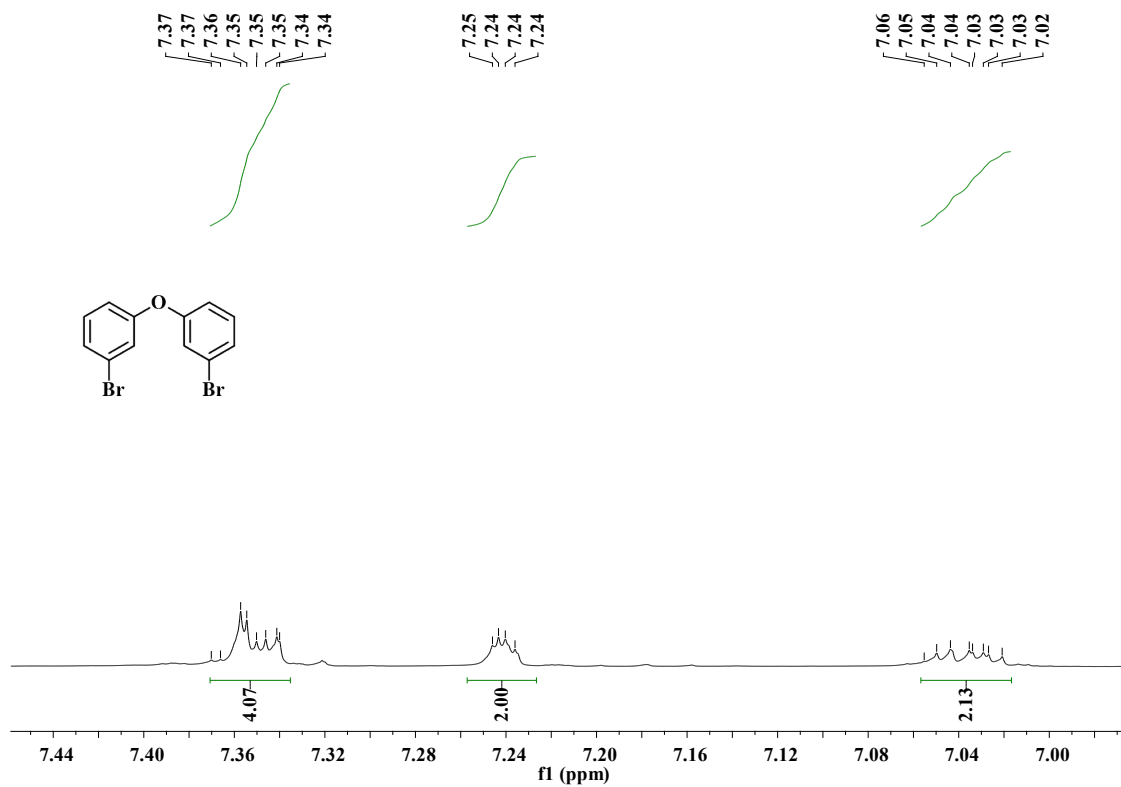


Fig. S14 ¹H-NMR spectrum of **obb** in DMSO (400 MHz)

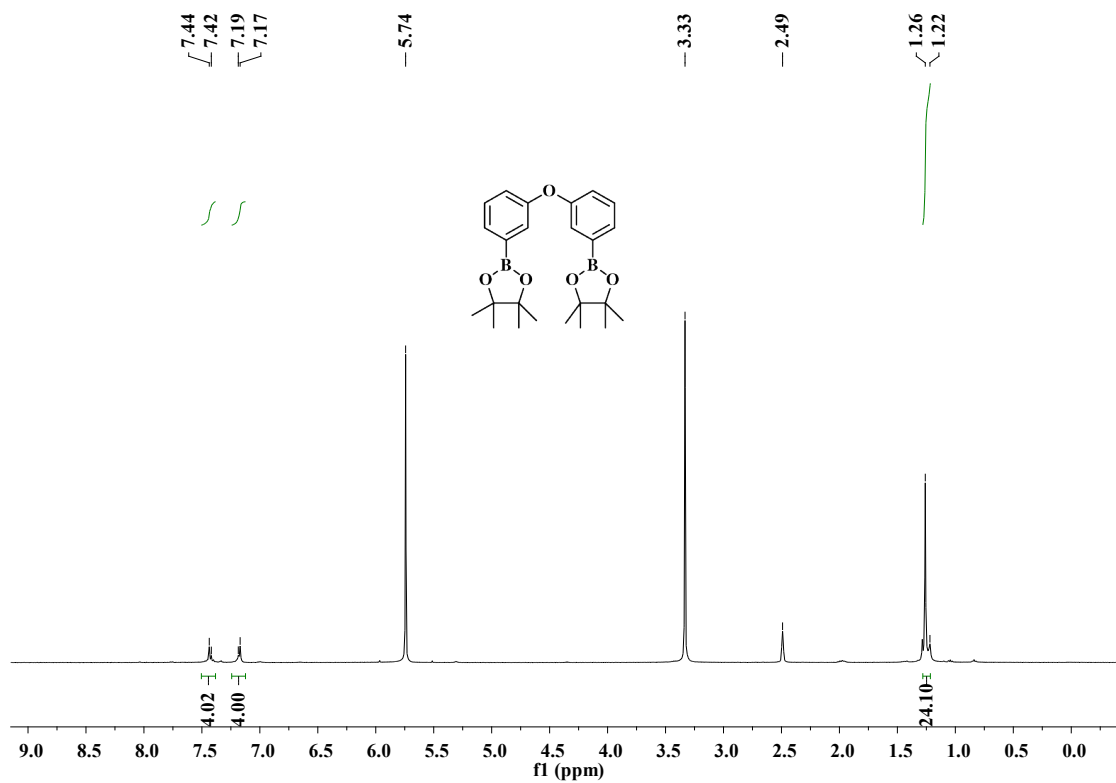


Fig. S15 $^1\text{H-NMR}$ spectrum of complexes **obp** in *DMSO* (400 MHz)

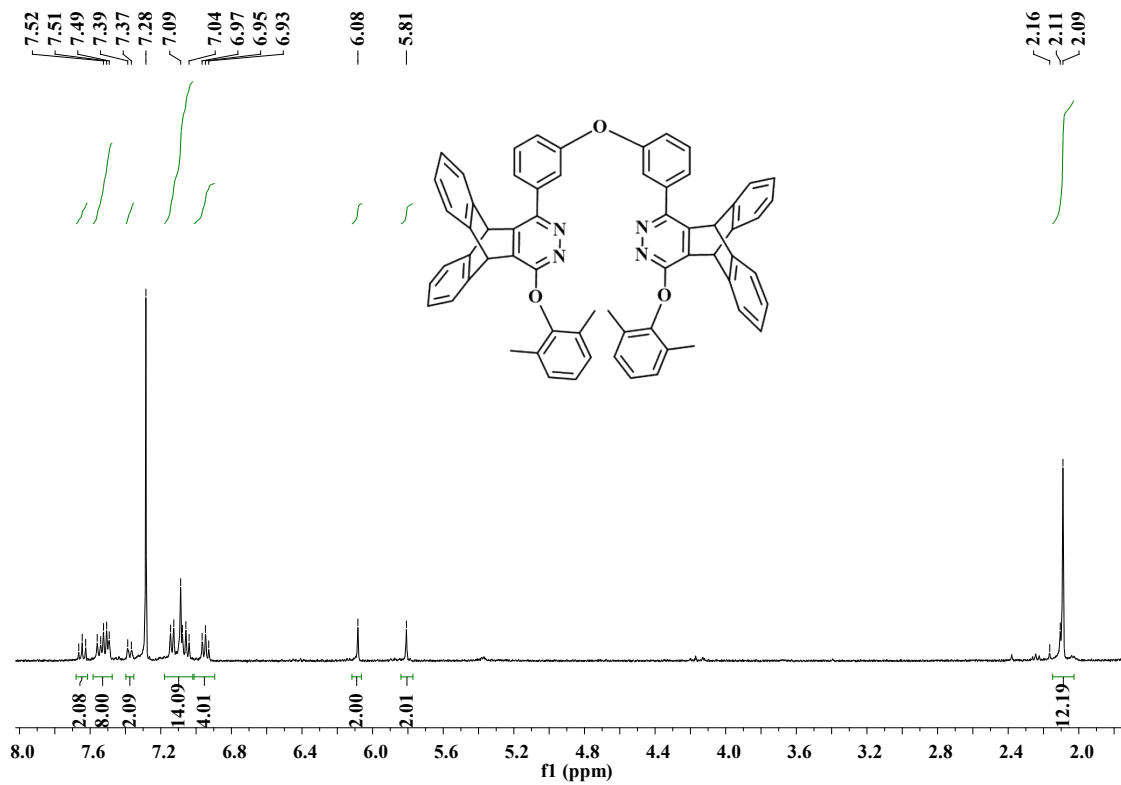


Fig. S16 $^1\text{H-NMR}$ Spectrum of complexes **ODPM** in *CDCl₃* (400 MHz)

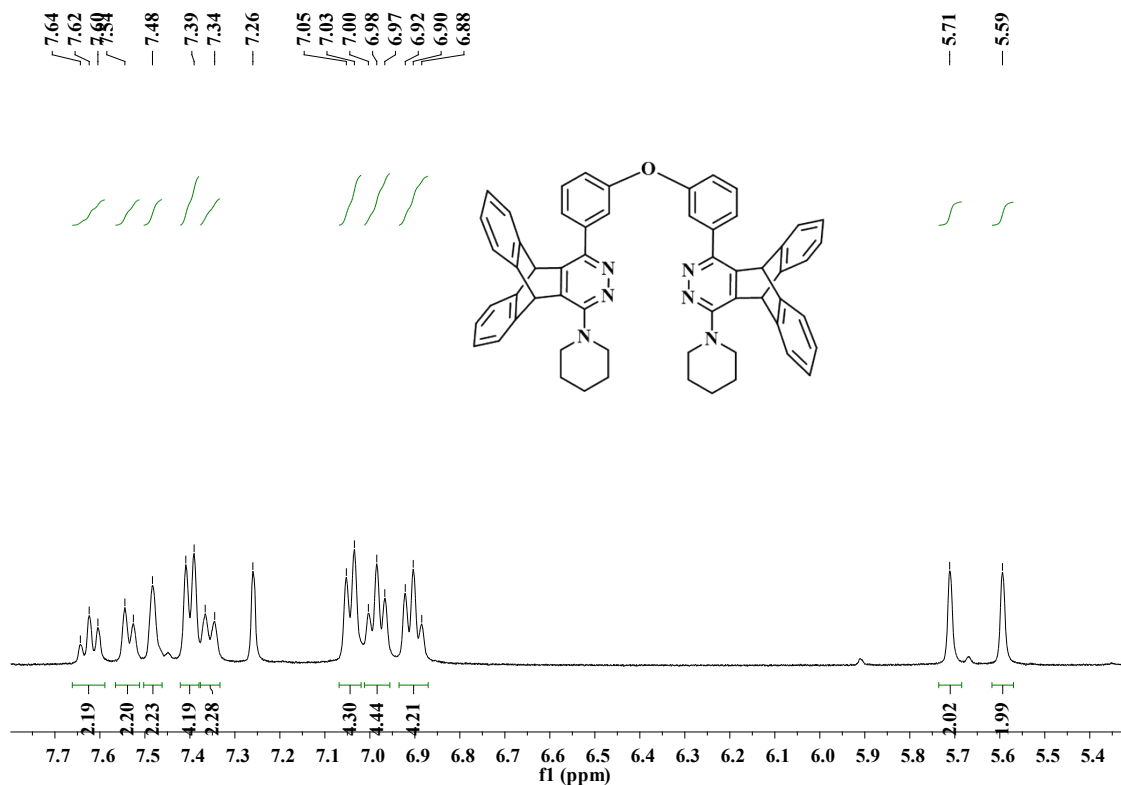


Fig. S17 $^1\text{H-NMR}$ Spectrum of complexes **OPIP** in CDCl_3 (400 MHz)

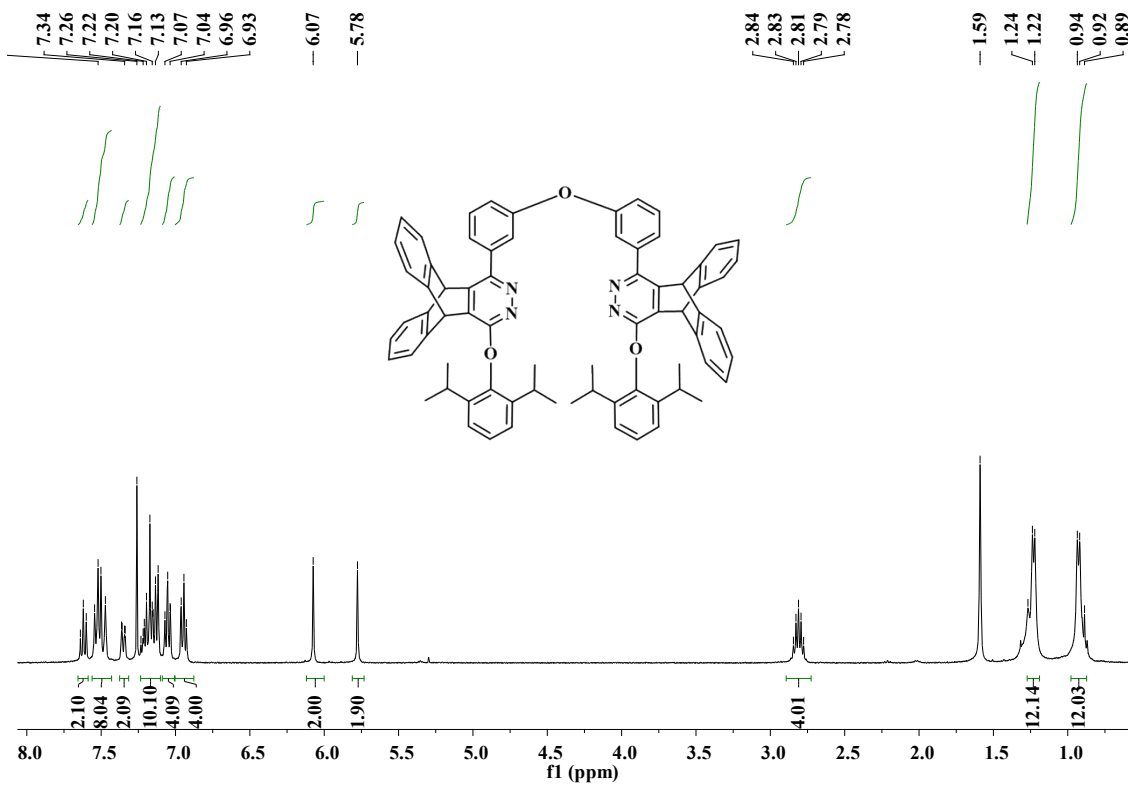


Fig. S18 $^1\text{H-NMR}$ spectrum of complex **ODPT** in CDCl_3 (400 MHz)

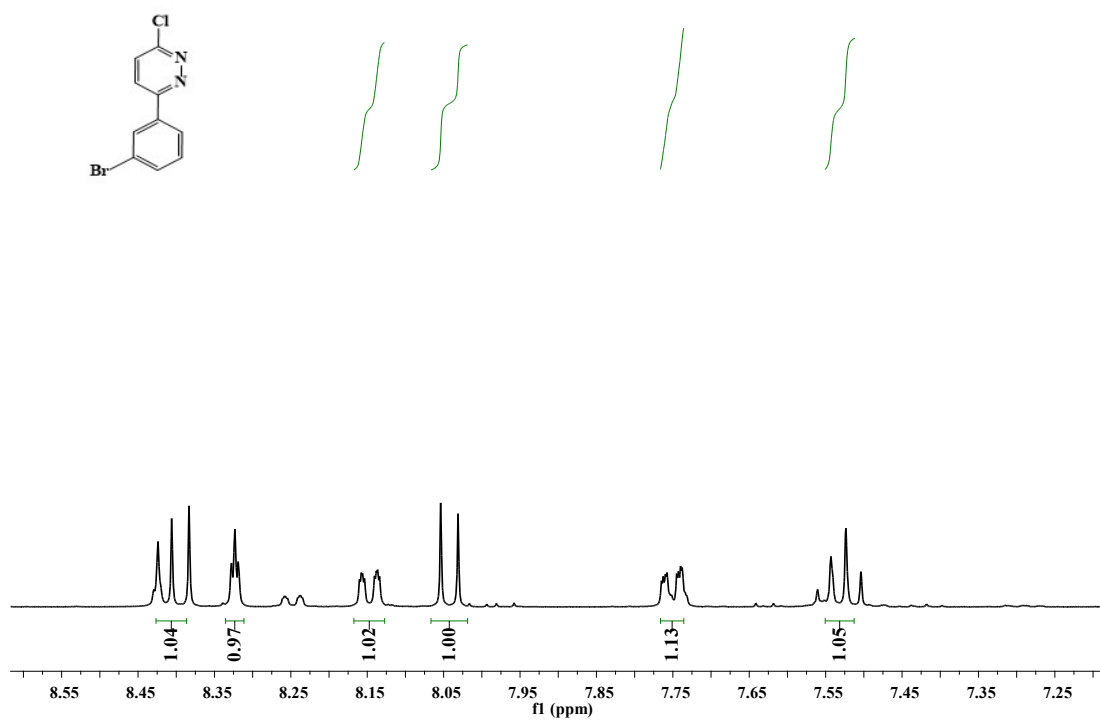


Fig. S19 $^1\text{H-NMR}$ spectrum of complexes **bcp** in *DMSO* (400 MHz)

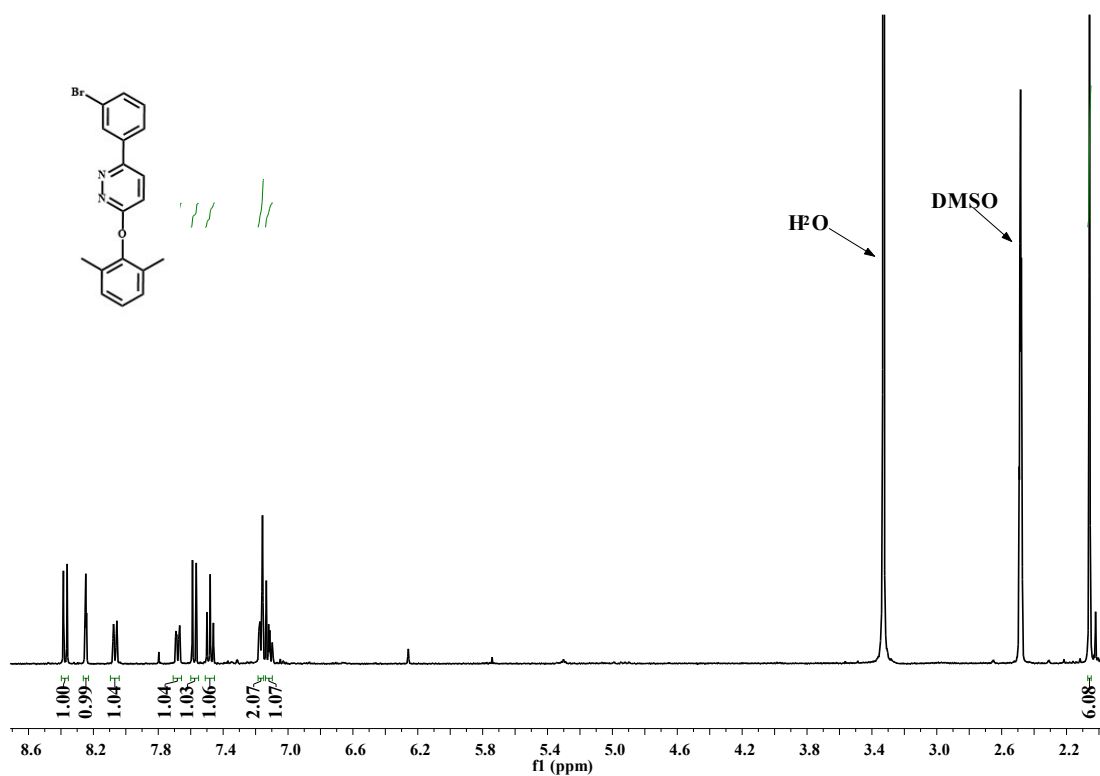


Fig. S20 $^1\text{H-NMR}$ spectrum of complexes **bdp** in *DMSO* (400 MHz)

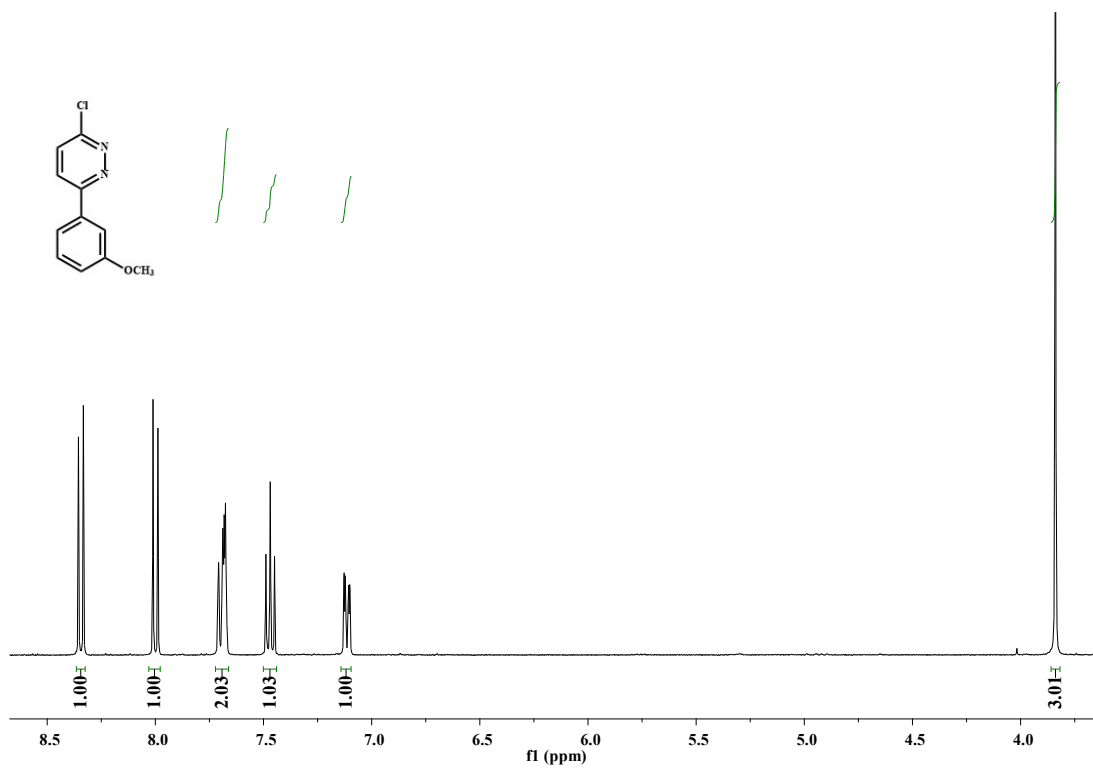


Fig. S21 ¹H-NMR spectrum of complexes **cmp** in DMSO (400 MHz)

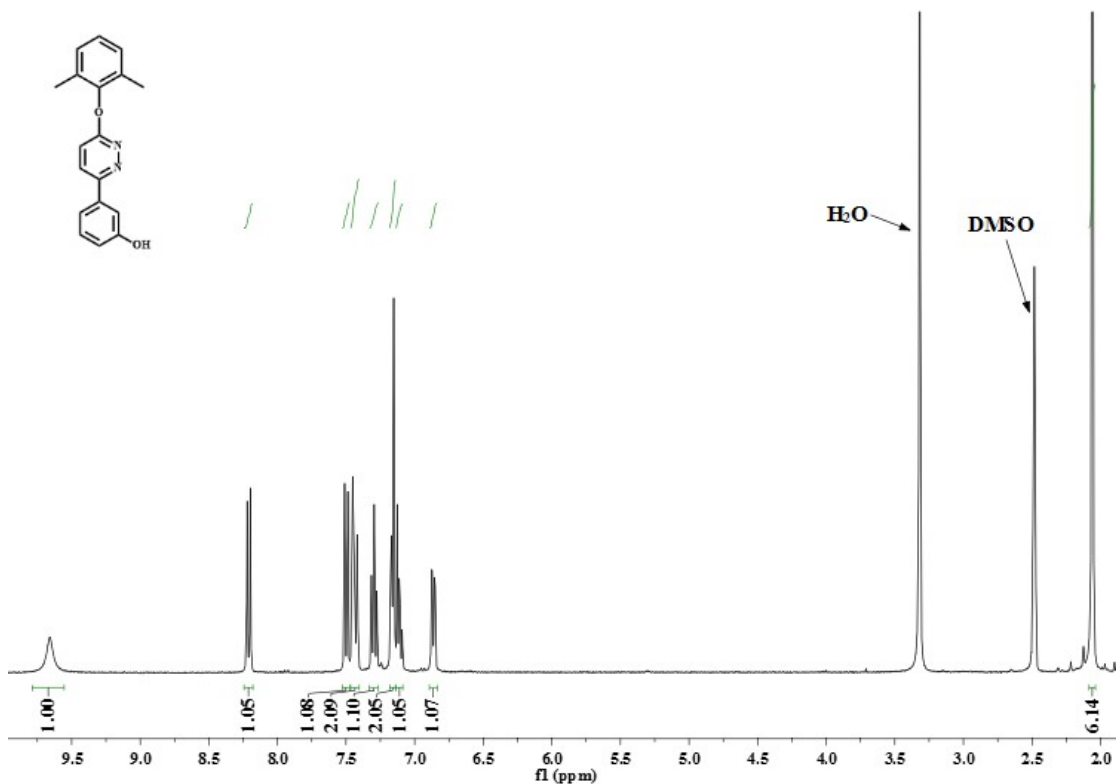


Fig. S22 ¹H-NMR spectrum of complexes **dpy** in DMSO (400 MHz)

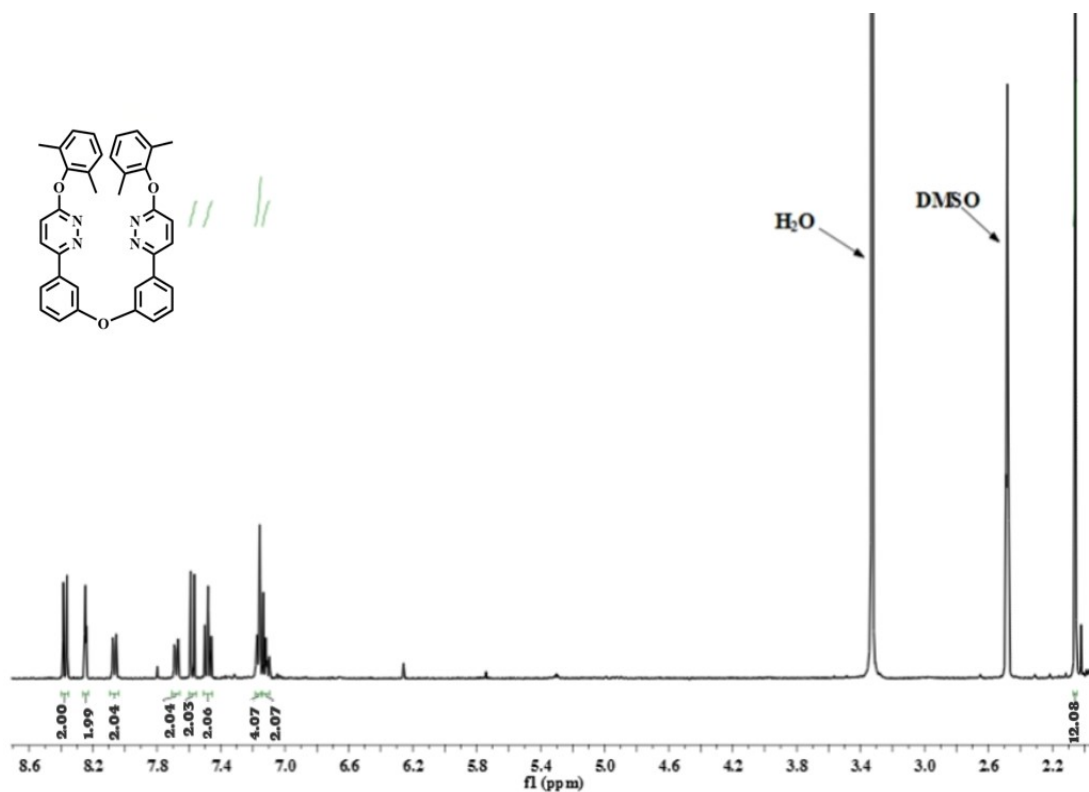


Fig. S23 ¹H-NMR spectrum of complexes **dp-o-dp** in DMSO (400 MHz)

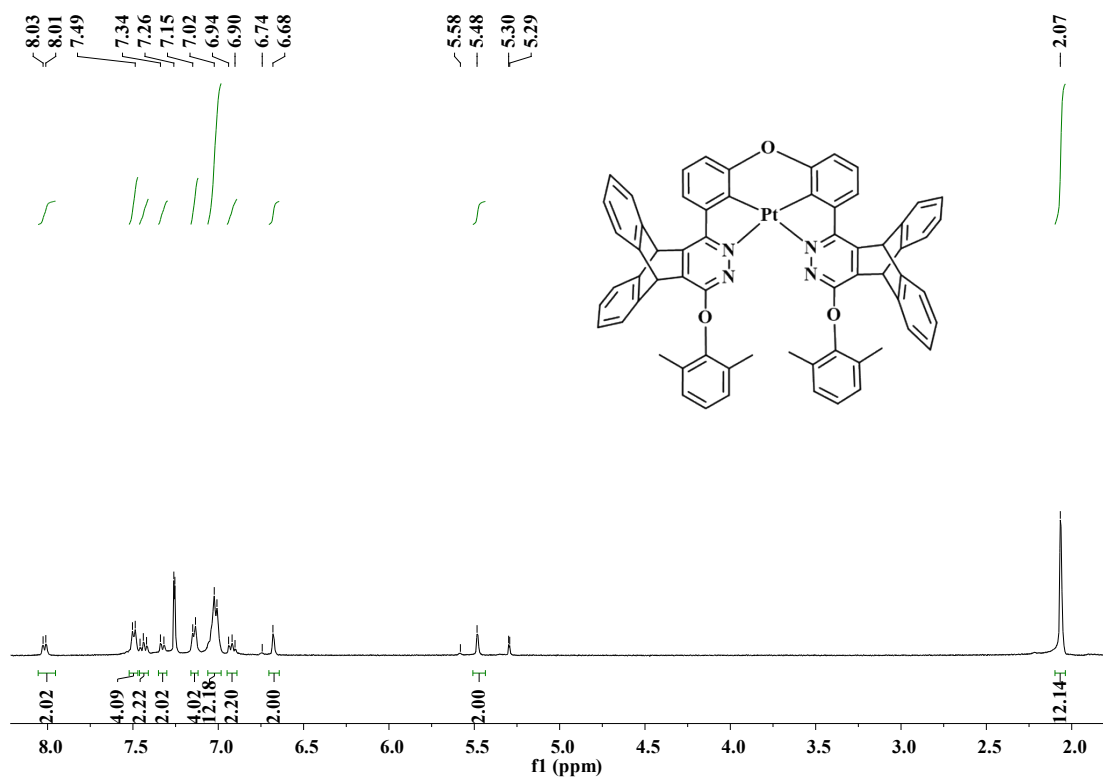


Fig. S24 ¹H-NMR spectrum of complex **Pt-DPM** in CDCl₃ (400 MHz)

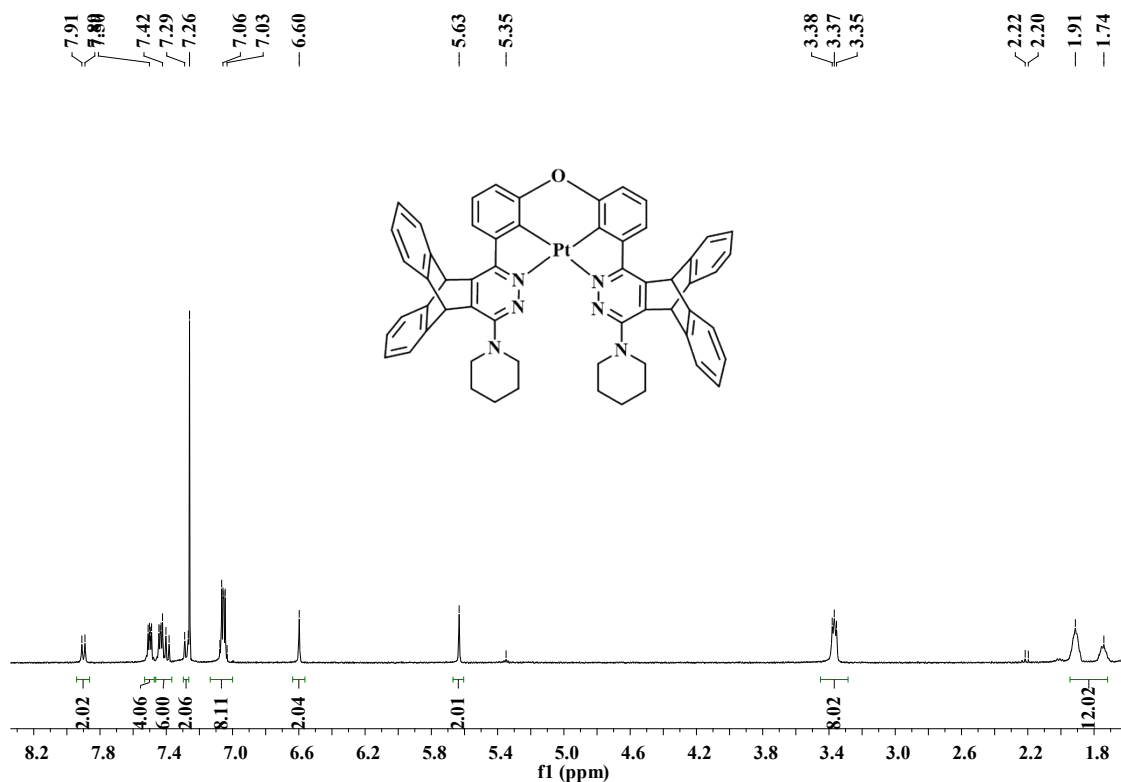


Fig. S25 ¹H-NMR spectrum of complex Pt-PIP in CDCl₃ (400 MHz)

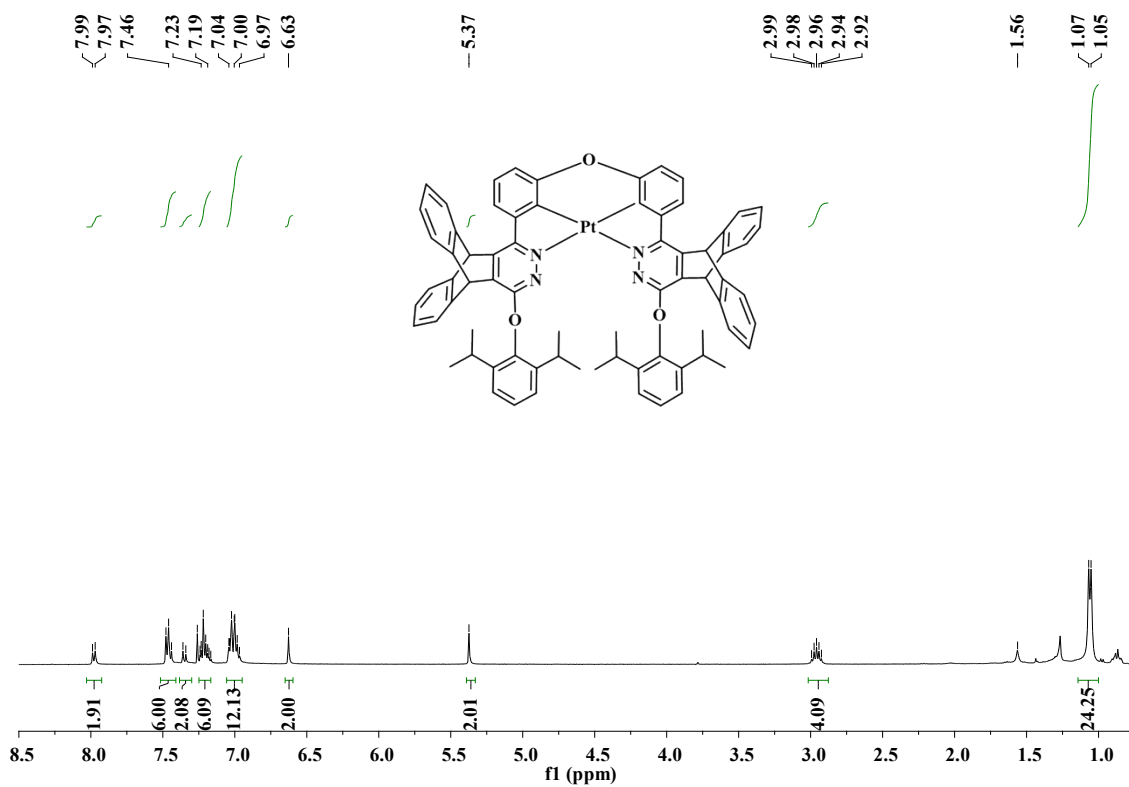


Fig. S26 ¹H-NMR spectrum of complex Pt-DPT in CDCl₃ (400 MHz)

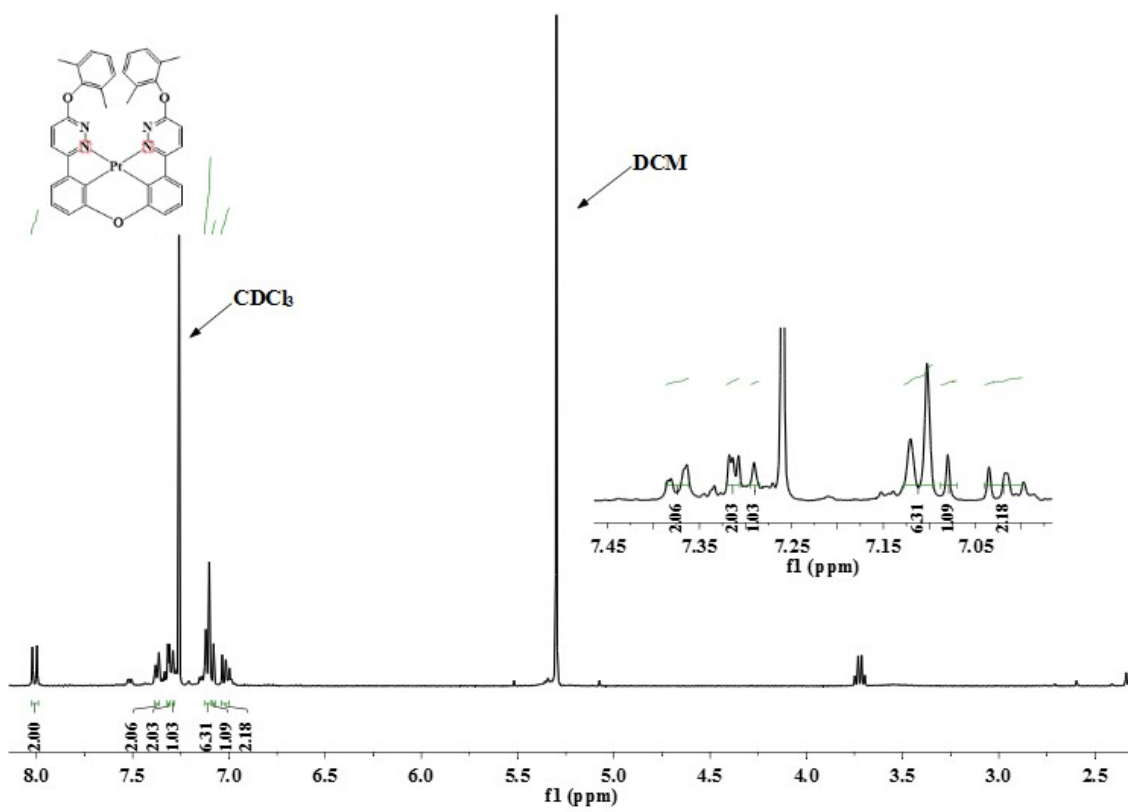


Fig. S27 $^1\text{H-NMR}$ spectrum of complex **Pt-D** in CDCl_3 (400 MHz)

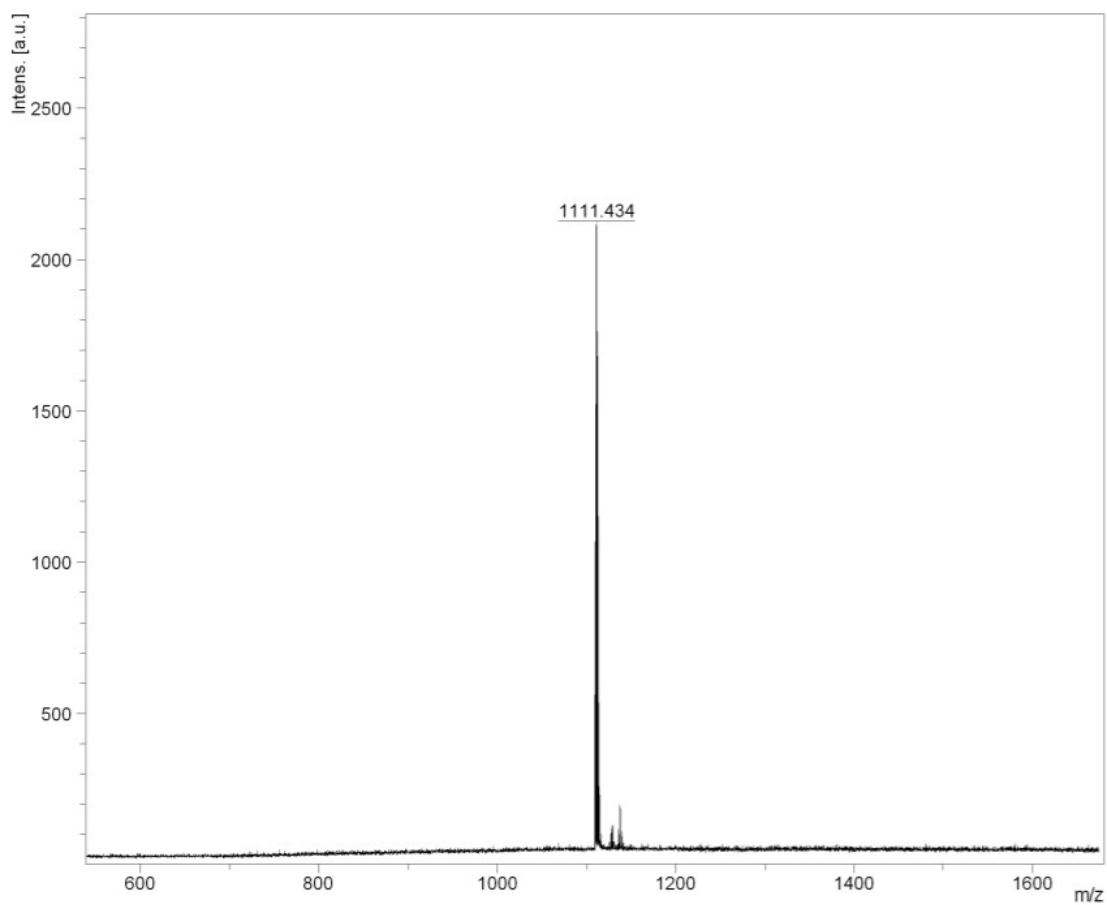


Fig. S28 MALDI-TOF Spectrum of compound **Pt-DPM**

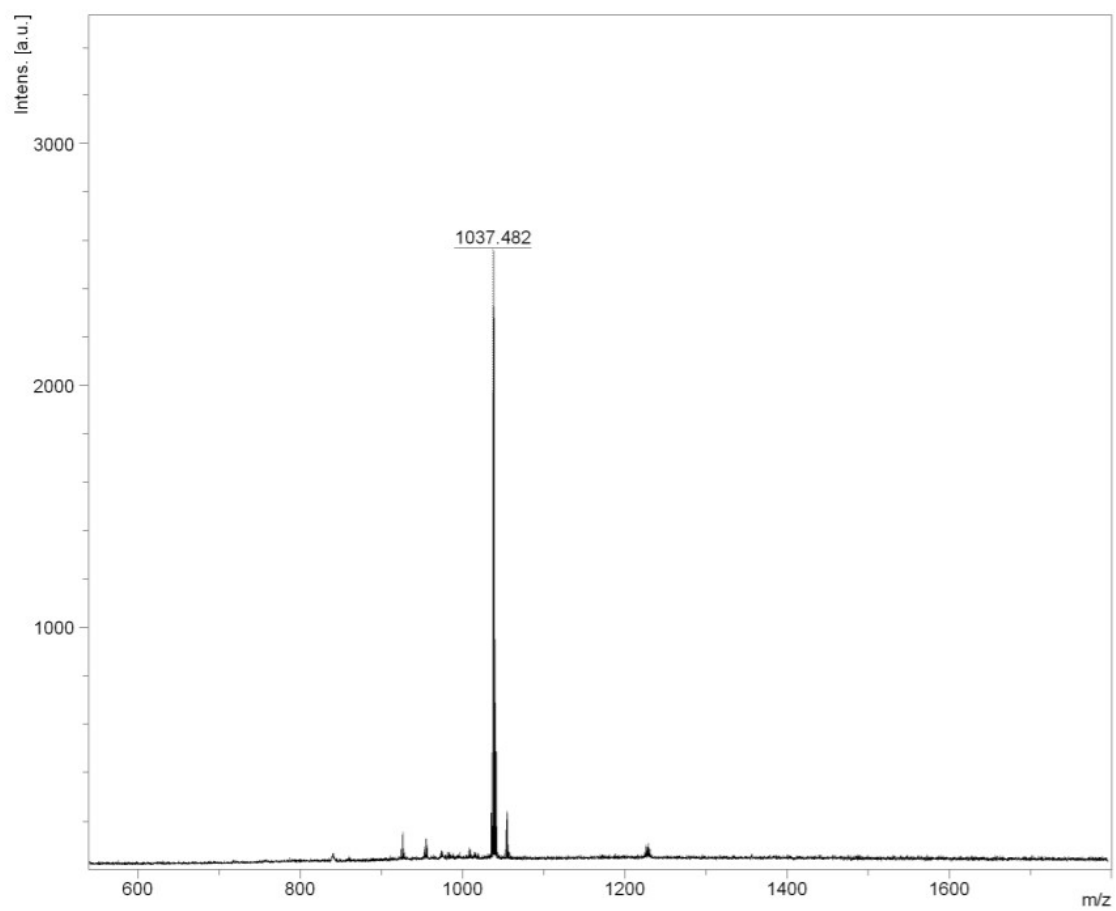


Fig. S29 MALDI-TOF Spectrum of compound **Pt-PIP**

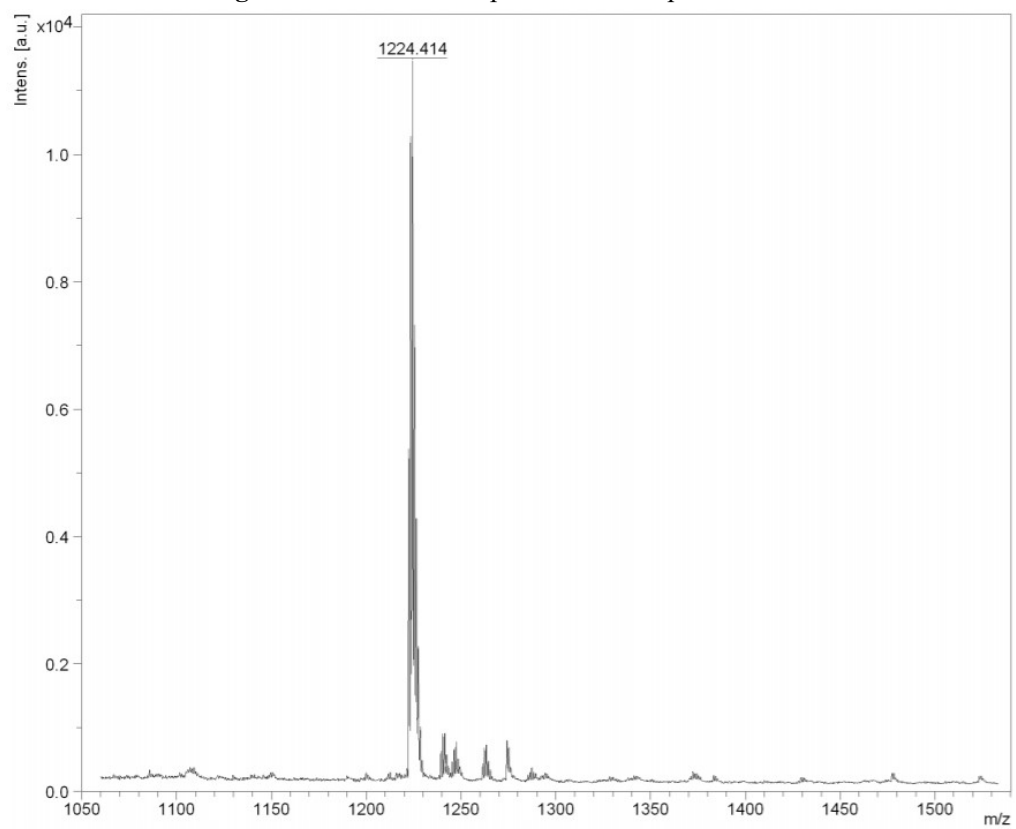


Fig. S30 MALDI-TOF Spectrum of compound **Pt-DPT**

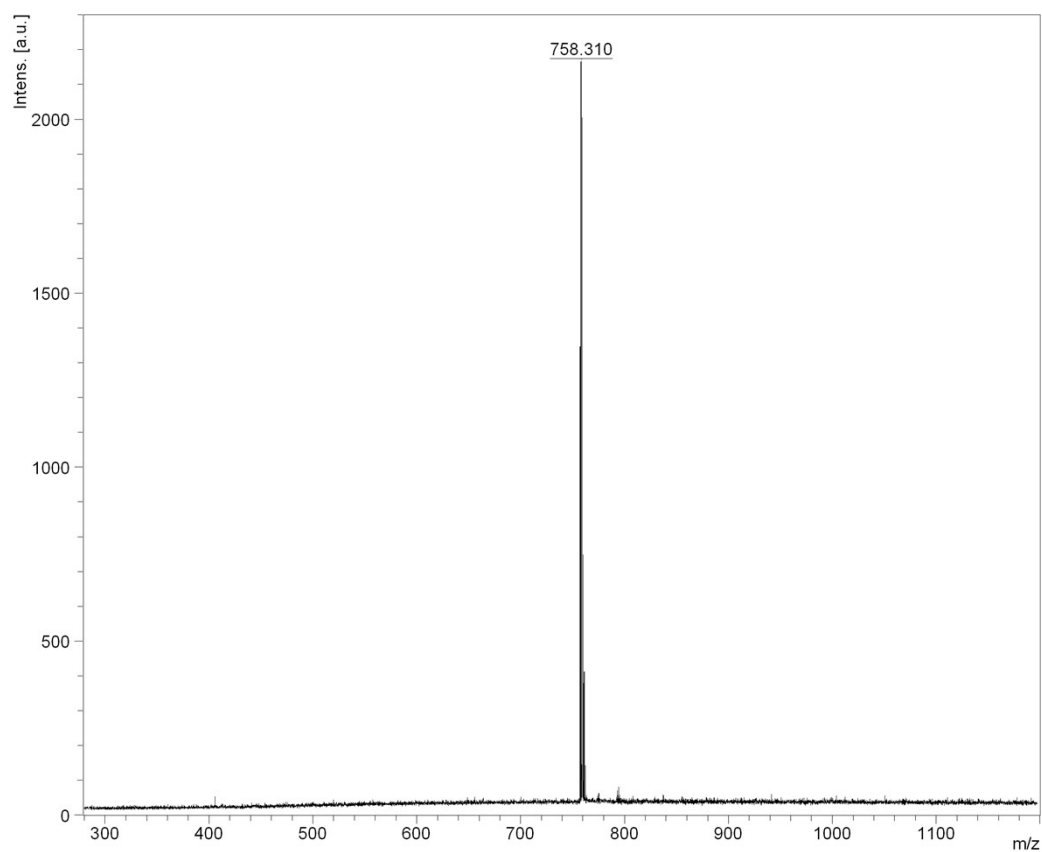


Fig. S31 MALDI-TOF Spectrum of compound **Pt-D**

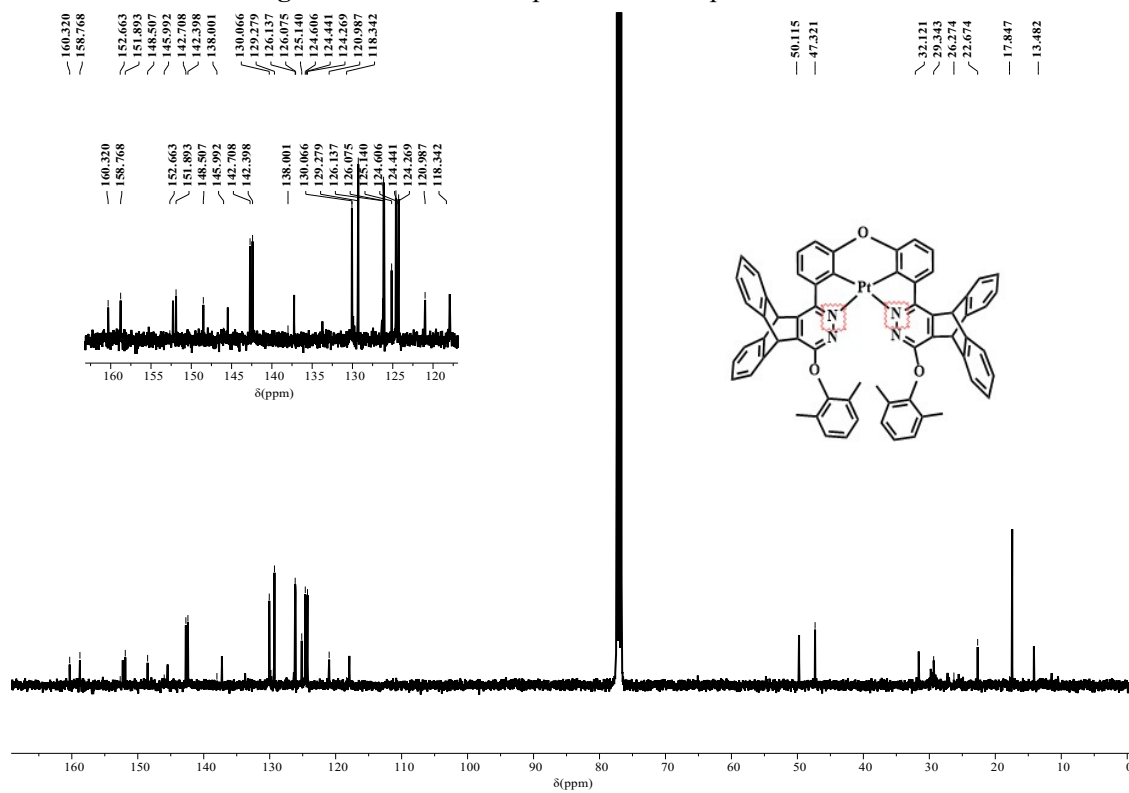


Fig. S32 ¹³C-NMR spectrum of complex **Pt-DPM** in $CDCl_3$ (100 MHz)

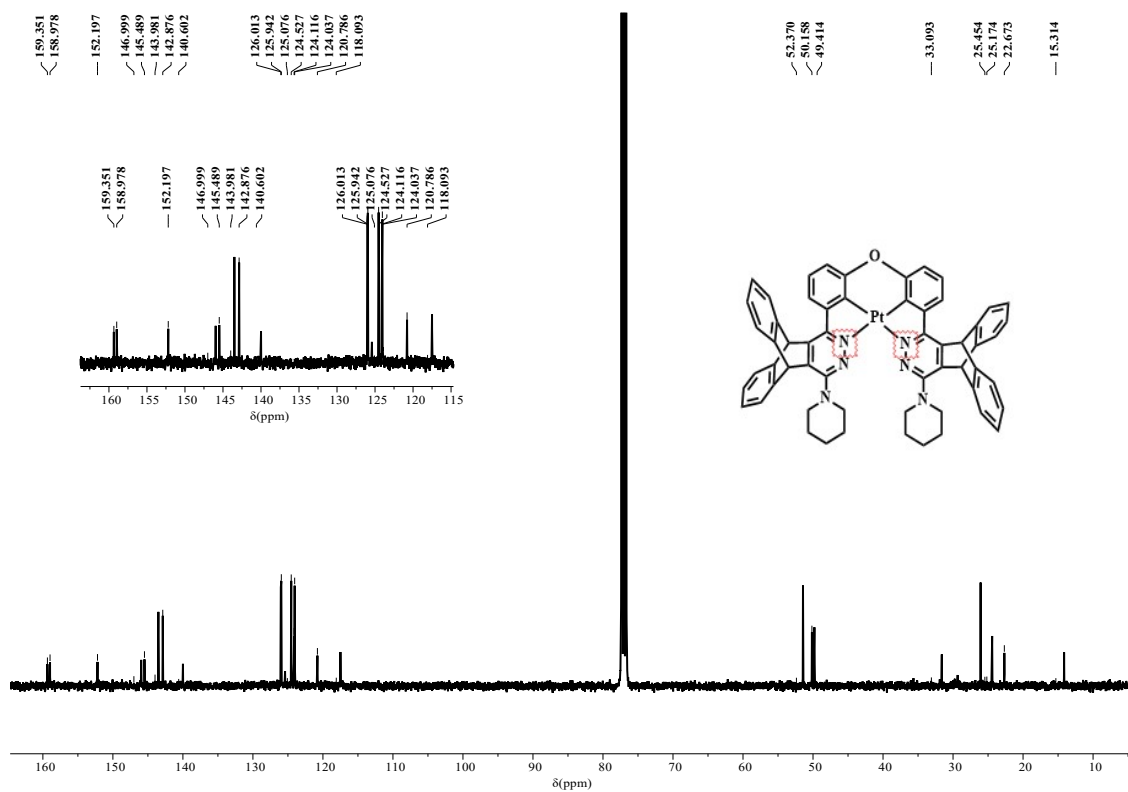


Fig. S33 ^{13}C -NMR spectrum of complex **Pt-PIP** in CDCl_3 (100 MHz)

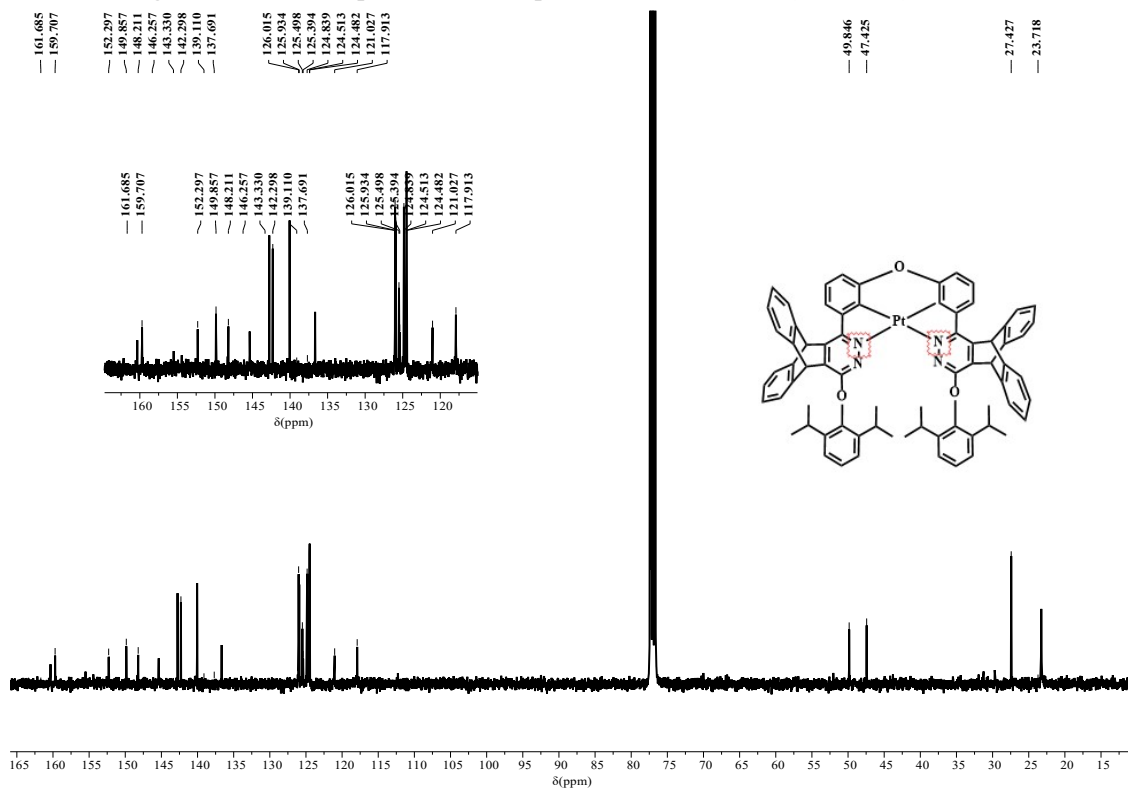


Fig. S34 ^{13}C -NMR spectrum of complex **Pt-DPT** in CDCl_3 (100 MHz)